

卢银, WETZLER Nadav, MARCO Shmuel, 等. 区域新构造活动的水下事件沉积响应: 以死海盆地和柴达木盆地为例[J]. 第四纪研究, 2022, 42(3):617-636.

LU Yin, WETZLER Nadav, MARCO Shmuel, et al. Subaqueous event deposits response to regional neotectonics: Case studies of the Dead Sea Basin and the Qaidam Basin[J]. Quaternary Sciences, 2022, 42(3):617-636.

doi:10.11928/j.issn.1001-7410.2022.03.01

文章编号: 1001-7410(2022)03-617-20

区域新构造活动的水下事件沉积响应: 以死海盆地和柴达木盆地为例*

卢银¹, Nadav Wetzler², Shmuel Marco³, 方小敏^{4,5}

(1. Department of Geology, University of Innsbruck, Innsbruck 6020, Austria; 2. Geological Survey of Israel, Jerusalem 9692100, Israel; 3. Department of Geophysics, Tel Aviv University, Tel Aviv 6997801, Israel; 4. 中国科学院青藏高原研究所, 青藏高原地球系统资源与环境国家重点实验室, 北京 100101; 5. 中国科学院青藏高原研究所, 大陆碰撞与高原隆升重点实验室, 北京 100101)

摘要:自 20 世纪 70 年代以来, 位于构造活跃区的盆地沉积序列的岩性、粒度与沉积速率的正向突变, 常被用来指示区域新构造活动。然而, 这种常规方法已经受到国内外学者强有力的质疑——用来推断构造活动的沉积学证据也可由气候因素引起。因而, 需寻找某种独立于气候因素的沉积学证据来可靠地指示新构造活动。震积岩, 由地震震动引起的、保存于湖相或海相地层序列中的事件沉积, 能可靠的指示区域新构造活动。新兴的交叉研究方向——湖泊/海洋古地震学, 通过研究保存于水下沉积序列中的震积岩, 可延长强震记录, 加深对断裂带活动性的认识。文章以死海盆地(中东地区)和柴达木盆地(青藏高原东北缘)为例, 从水下事件沉积响应的视角, 借助超长尺度的震积岩序列, 理解千年-构造尺度上的区域新构造活动特性。基于死海湖心 457 m 长的 ICDP 5017-1 岩芯保存的震积岩序列, 我们建立了一条由 151 个 $M_w \geq 7$ 地震事件组成的, 全球最长的(220 ka)连续大地震记录, 该记录揭示了缓慢滑动的死海断裂带上的大地震具有聚类式的复发特征, 以及不同断层分支相互作用、聚类活动的模式; 基于青藏高原东北缘柴达木盆地西部的碱山背斜顶部 SG-1b 岩芯上部 260 m 沉积序列, 我们建立了一条由 164 个震积岩层位构成的覆盖 3.6~1.6 Ma 的震积岩序列, 该序列在 3.6~2.7 Ma 时段内相对较为连续, 由 126 个地震事件和 5 个地震集合组成, 揭示了与强烈区域变形有关的晚上新世幕式逆冲过程。

关键词:震积岩; 湖泊/海洋事件沉积; 湖泊/海洋古地震学; 强震复发模式; 区域新构造活动特性

中图分类号: P546

文献标识码: A

开放科学标识码(OSID)



0 引言

新构造运动, 一般指新第三纪(中新世)23 Ma 以来发生的地壳运动。新构造活动的表现形式包括: 长时间尺度上的板块运动、中-短尺度上的火山活动及地震等^[1]。其中, 地震因分布范围广、复发周期相对较短等特点, 最具有破坏性^[2-4]。长久以来, 基于新构造活动引起的山地剥蚀-盆地沉积效应^[5-7], 位于构造活跃区的盆地沉积序列的岩性、粒度与沉积速率的正向突变(增粗或增高), 常常被用来指示区域新构造活

动^[8-17]。然而, 这种常规的解释方法已经受到国内外研究者强有力的质疑——用来推断构造作用的沉积学证据也可以由气候因素引起^[18-21]。

由于构造活动^[5,14]与大幅度气候变化^[19,21]都可以导致山地剥蚀增强、盆地沉积速率增加, 常规的岩性、粒度与沉积速率等指标皆为混合性指标。因而, 并不能可靠、有效地反演区域新构造活动历史。我们需要寻找某种独立于气候变化因素的沉积学证据, 来可靠的指示新构造活动。震积岩(seismites)——由地震震动引起的、保存于湖相或

2021-11-26 收稿, 2022-01-28 收修改稿

* 科技部第二次青藏高原综合科学考察研究项目(批准号:2019QZKK0707)、中国科学院(A类)战略性先导科技专项项目(批准号:XDA20070201)和奥地利科学基金会项目(批准号:Austrian Science Fund;M 2817 to Yin Lu)共同资助

第一(通讯)作者简介: 卢银, 男, 34 岁, 项目研究员, 海洋/湖泊古地震学, E-mail: yinlusedimentology@yeah.net 或者 yin.lu@uibk.ac.at; 获 2022 年欧洲地球科学联合会(EGU)地层学、沉积学、古生物学领域“青年科学家奖”

海相地层序列中的事件沉积^[22-26],能可靠地指示区域新构造活动。在国内,震积岩研究相对薄弱,已有的研究主要集中在非常古老的、常遭受后期漫长构造运动改造的地层,不利于排除区域构造应力对事件沉积的影响^[25,27-30];同时,缺乏对考古、历史和器测时期(3~0 ka)湖泊/海洋沉积序列中震积岩的详细研究,无法将事件沉积与考古、历史和器测强震事件进行高精度对比,从而无法可靠地建立震积岩标志。此外,缺乏对构造活跃区湖泊/海洋现代沉积过程的充分理解,难以排除非地震因素或沉积动力对目标事件沉积层的影响。因而,国内已有的震积岩研究常常受到地学界同行的质疑。

震积岩,是新兴交叉研究方向——湖泊/海洋古地震学(Lacustrine/Marine Paleoseismology)的主要研究对象。湖泊/海洋古地震研究^[31-34]与陆地探槽古地震研究^[35-37]、树轮古地震研究^[38-39]、洞穴沉积古地震研究^[40-41]以及考古古地震研究^[42-43]等,具有相同的目标——从各种地质记录中识别地震事件,确定地震发生时间,推测地震烈度、震级,探讨发震断层的地震重现模式和区域多断层间的相互作用(如应力转移)等^[44]。保存且反复出现于连续的、时间分辨率较高的、超长尺度的湖泊/海洋沉积序列中的震积岩,可以极大的延长强震记录;通过对震积岩(如原位软沉积变形结构)形成过程的定量流体数值模拟,可以帮助限定古地震烈度与震级^[32],从而加深我们对千年-构造尺度断裂带活动性的认识^[32,45-47]。本文以湖泊/海洋古地震学研究的经典地区——死海盆地和青藏高原北部柴达木盆地为例,从水下事件沉积响应的视角,借助超长尺度的震积岩序列,理解千年-构造尺度上的区域新构造活动特性。本文所使用的“震积岩”,包含由地震震动驱动的原位沉积与异地搬运沉积。

本文基于已发表于国际英文期刊的两项研究:(1) Lu, et al., 2020, Science Advances (Open Access; CC BY-NC 4.0)^[32]; (2) Lu, et al., 2021 (March), Geophysical Research Letters (Open Access; CC BY 4.0)^[46]。因而,本文部分细节内容可视为前述两项研究的中文翻译版。上述2篇文献均为开放获取,允许被翻译与再编辑使用,并在本文已被合适的引用与标注,特此说明。

1 地质背景、研究材料与年代

1.1 死海盆地与国际大陆钻探(ICDP)5017-1岩芯

死海断裂带(Dead Sea Fault)是一条长度

>1000 km、位于非洲板块和阿拉伯板块之间的左旋走滑板块边界(图1A),年均滑动速率<5 mm,是东非大裂谷向北的延伸,也是地球上最著名的发震断层之一^[48-49]。它与美国西部圣安德烈亚斯断裂带(San Andreas Fault)^[35,37,50]、新西兰阿尔卑斯断裂带(Alpine Fault)^[45,51-52]及青藏高原阿尔金断裂带(Altyn Tagh Fault)^[36,53-54]均为全球研究程度最高的大型走滑断层。死海盆地位于死海断裂带中部(图1B),是该断裂带上最大、最深的大陆拉分盆地。该盆地南-北长约150 km,东-西宽约15 km,自第四纪以来其沉积中心(即死海湖心)接受了约4 km厚的湖相沉积^[49]。死海盆地第四纪以来被不同大小的水体占据:Amora湖(Q₁~MIS6)、Samra湖(MIS5)、Lisan湖(MIS4~2)及现今的死海(MIS1)^[55-56]。其中,末次冰盛期的Lisan湖南-北长约240 km,湖面海拔高度为-180 m,是该盆地所知的最大的湖泊系统^[57-58]。现今,死海流域面积约43000 km²,自北向南气候带依次为湿润-半湿润的地中海气候、半荒漠气候及荒漠气候^[59]。年均降水量由流域盆地最北部(叙利亚)的1000 mm降至最南部的10 mm^[60]。该区域夏半年(4~9月)是干旱期,冬半年(10月~次年3月)是湿润期。

死海是全球地表最低的地方,海拔-437 m,与其东、西部山地和高原高差>1500 m,其水体具有超高的含盐度(240 g/L)。国际大陆钻探计划(ICDP)于2010~2011年期间,在300 m水深之下的死海中心实施了钻探^[67]。该钻孔(ICDP 5017-1)(31°30'29"N, 35°28'16"E)深457 m,平均取心率为88%(图1B和1D)。该沉积序列由白色文石-褐色泥质碎屑交替纹层(aragonite-detritus laminae)、石盐、石膏、均质泥岩、浊流沉积、水下泥石流沉积及水下滑塌沉积这7种基本岩相构成^[26,68-71];其中,石盐与石膏分别主要出现在间冰期及冰期的间冰阶,指示相对干旱的气候^[69,72]。白色文石-褐色泥质碎屑交替纹层指示相对湿润的气候^[73-75],其中褐色泥质碎屑层由粉砂粒级的石英与方解石颗粒组成,主要沉积于湿润的冬半年;而白色文石层主要沉积于干旱的夏半年^[76-78]。详细的¹⁴C^[65]与U-Th^[69]定年以及 $\delta^{18}\text{O}$ 地层比对^[66]揭示,死海ICDP 5017-1岩芯沉积序列的年代范围为220~0 ka(图1D),死海中心年均沉积速率为2 mm。

1.2 柴达木盆地(西部)与中-德碱山SG-1b岩芯

柴达木盆地是青藏高原最大的盆地,其形成受

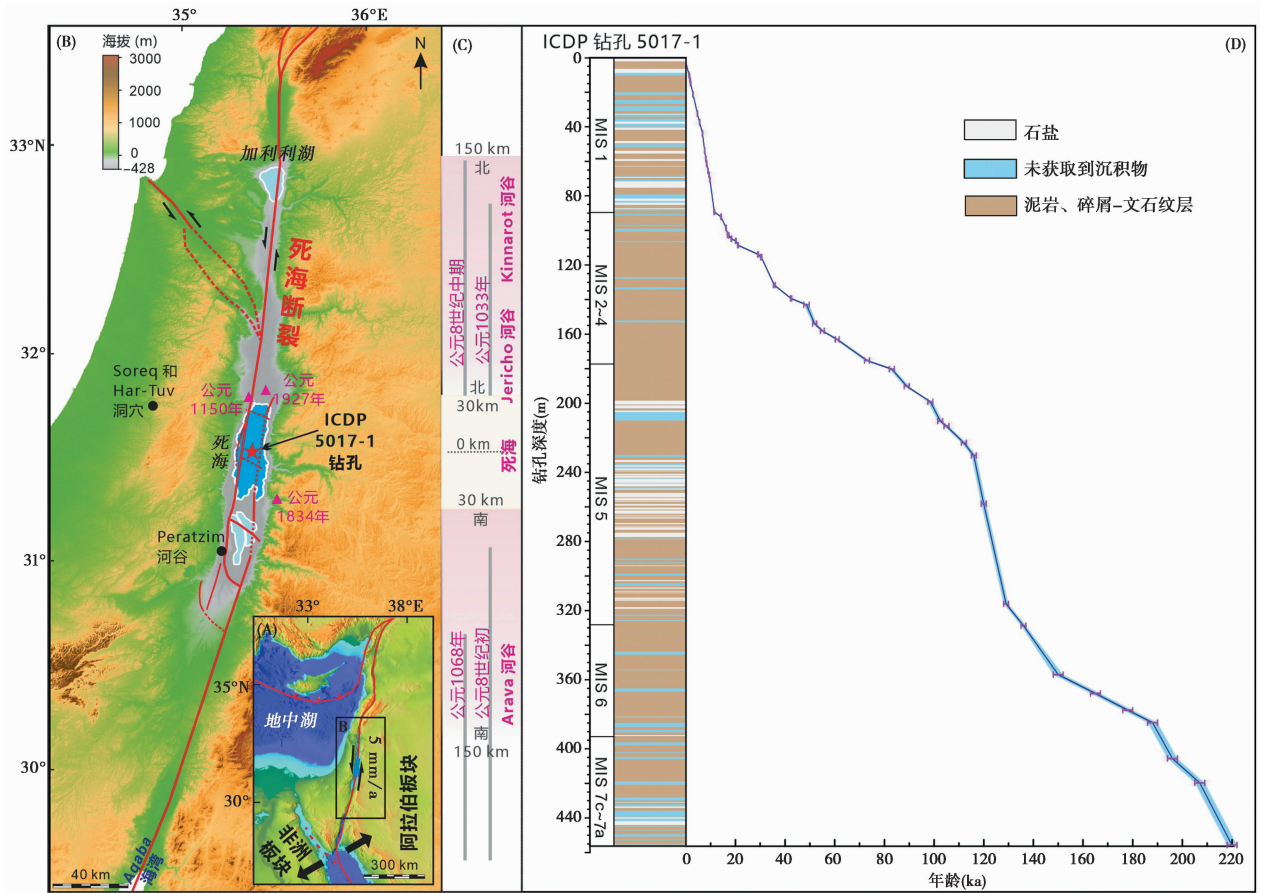


图 1 死海断裂带构造背景与历史、器测强震($M_w \geq 6$)分布及 ICDP 5017-1 岩芯概况(修改自 Lu 等, 2020^[32])
 (A)死海断裂带构造背景^[49]; (B)断层分布^[49,61]及过去 2000 年发生于 ICDP 5017-1 钻孔附近的 $M_w \geq 6$ 地震(红色三角形)^[62];
 (C)公元前 31 年以来发生于死海断裂带中部(钻孔南、北沿死海主断层 150 km 范围内)的 $M_w \geq 7$ 地震^[63-64],其中,灰色线段代表
 主断层地表破裂范围;(D)死海 ICDP 5017-1 岩芯年代模型^[65-66]

Fig. 1 Tectonic setting of the Dead Sea Fault and the ICDP Core 5017-1(modified from Lu et al., 2020^[32]). (A) Location of the Dead Sea Fault^[49]; (B) Major active faults^[49,61] along the plate boundary and historic and instrumental $M_w \geq 6$ earthquakes (red triangles)^[62] near the drilling site during the past 2000 a; (C) Fault rupture (gray lines) of historic $M_w \geq 7$ earthquakes since 31 BC^[63-64] that occurred along the focused part of the fault—The central Dead Sea Fault (up to 150 km north and south of the drilling site); (D) Age model of the ICDP Core 5017-1^[65-66]

到新生代印度-亚欧板块碰撞的强烈影响^[79-80]。该盆地现今范围西北至阿尔金山脉,南至昆仑山脉,东北至祁连山脉,总面积约 120000 km²^[79,81-82](图 2A~2B),接受了厚达 12 km 的新生代沉积^[83-84]。盆地内部平均海拔约 2800 m,与周边山脉高差 >2000 m,气候以极低的降水量(年均值 <50 mm)、极高的潜在蒸发量(年均值约 3000 mm)和强风为特征^[85]。渐新世-第四纪期间,青藏高原持续的向东北方向生长及伴随的沿昆仑山断裂带传播的地壳变形,形成了一系列沿阿尔金断裂带分布的褶皱(逆冲断层、背斜)^[80,86-89]。这些褶皱呈现近乎平行的南北-东西走向,沿着阿尔金断裂带延

伸数百千米,构成了柴达木盆地最显著的形貌特征(图 2B)以及 GPS 速率分布^[90],并在该区中新世-第四纪隆起中起着重要作用。

柴达木古湖泊于渐新世开始出现于该盆地西部^[91],在中新世气候湿润期得到扩展,最后在上新世-更新世期间因区域隆升与气候干旱化而萎缩、消失^[79,83-84]。柴达木古湖泊沉积了一套连续的湖相沉积序列,连续地记录了由印度-亚欧板块碰撞驱动的下伏逆冲断层的活动历史。详细的地震反射剖面显示,上述褶皱带中的碱山背斜,与柴达木古湖泊底部渐新世发育的隐伏逆冲断层相关^[92],自中新世以来经历了加速构造变形^[86,93-95]。

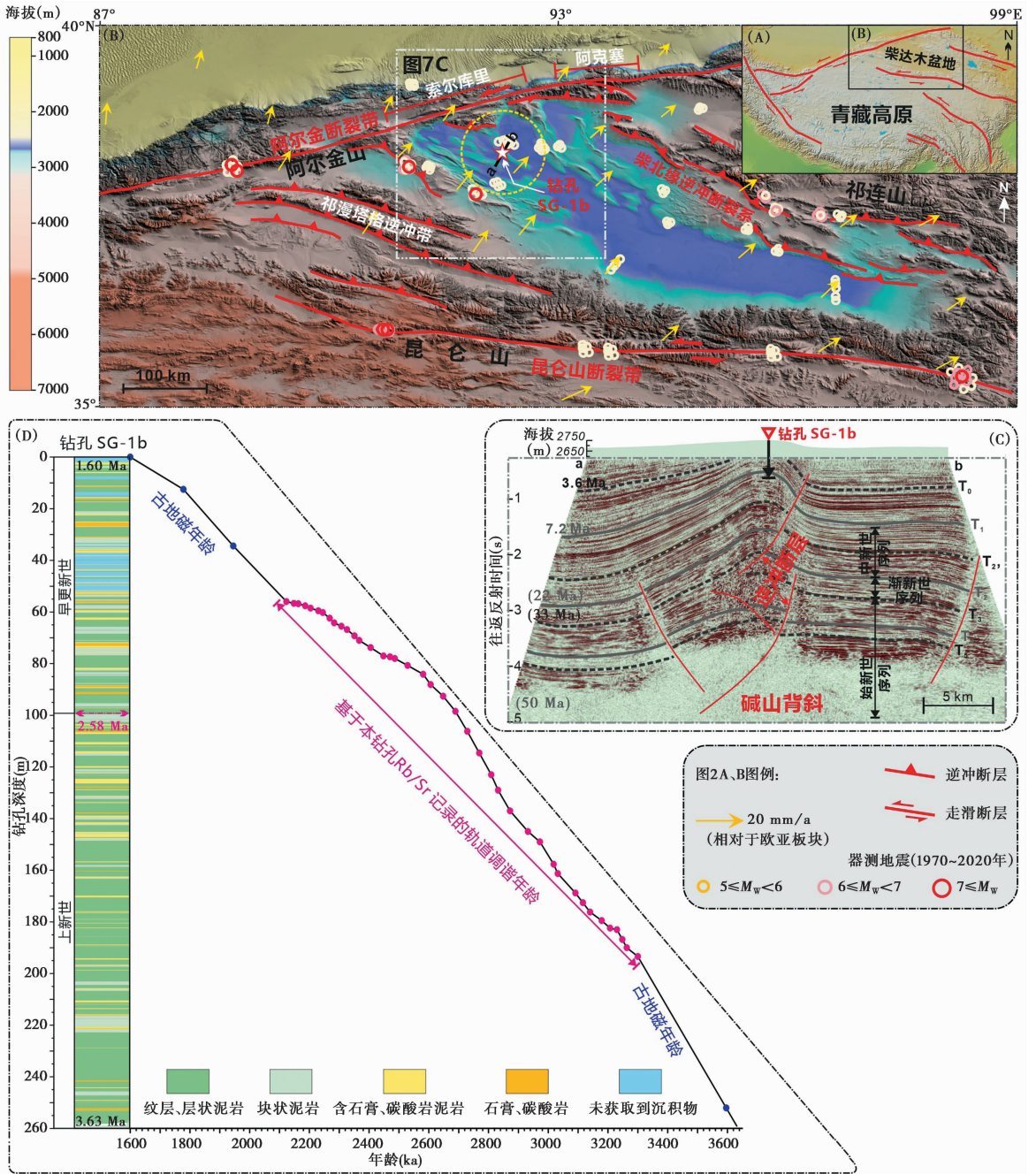


图 2 研究区地质背景、器测中-强震 ($M_w \geq 5$) 分布及 SG-1b 岩芯概况 (修改自 Lu 等, 2021^[46])

(A) 柴达木盆地位置与青藏高原大型断裂带分布^[81-82]; (B) 研究区活动断层^[53,81]、GPS 速率分布^[90]及 1970~2020 年中-强震分布 (<http://ds.iris.edu/ds/>); (C) 过碱山背斜和 SG-1b 钻孔的地震反射剖面 (图 2B 里的线 a-b) (修改自 Lu 等, 2015^[92]); (D) 柴达木盆地西部 SG-1b 岩芯 0~260 m 岩性与年代模型^[46,97-98]

Fig. 2 Geological setting of the study area and Core SG-1b (modified from Lu et al. , 2021^[46]). (A) Location of Qaidam Basin and major faults on the Tibetan Plateau^[81-82]. (B) Active faults^[53,81], GPS velocity^[90] and earthquakes during the years 1970~2020 (<http://ds.iris.edu/ds/>) in the region. (C) Seismic profile (line a-b in Fig. 2B) across the Jianshan Anticline (modified from Lu et al. , 2015^[92]); (D) Age model of Core SG-1b^[46,97-98]

2010 年至 2011 年期间, 中-德联合钻探项目在碱山背斜顶部钻取了 723 m 深的 SG-1b 孔 (38°21'9.46"N, 92°16'24.72"E) (图 2C)。该沉积序列主要由含粘土纹层的泥岩、均质泥岩、含

中-粗粉砂层的泥岩、层状粗粉砂岩、含蒸发岩碎屑的泥岩、富含鲕粒的泥岩、含泥蒸发岩等 7 种基本岩相组成^[96]。古地磁定年将该序列年代限定在 7.3~1.6 Ma^[97]。本研究聚焦于 SG-1b 岩芯上部

260 m。详细的古地磁定年^[97]及基于 Rb/Sr 记录的轨道调谐^[98]将其年龄限定在 3.6~1.6 Ma(图 2D)。

2 古地震事件的水下沉积响应——震积岩

2.1 死海盆地典型震积岩

2.1.1 死海震积岩研究历史

死海盆地所处的特殊地质背景(图 1A)、极高的湖相沉积速率(2 mm/a)及独特的文石-泥质碎屑交替纹层沉积^[68-69,74-75],使得盆地中心连续堆积的饱和水的松软泥质沉积物成为强震的绝佳记录器。特别是白色文石-褐色泥质碎屑交替纹层,非常有利于从沉积序列里识别出由地震震动形成的沉积结构^[26]。德国著名地质学家 Adolf Seilacher(图宾根大学,曾于 1969 年正式提出术语“seismite”^[23]) 在 1984 年,首先推测保存于死海东部湖岸剖面末次冰期沉积序列中的不对称褶曲(asymmetric folds)是地震震动触发的软沉积变形结构^[22];随后,约旦地质学家对这些变形结构进行了更详细地观察与描述^[99]。

20 世纪 80 年代末期,以色列希伯来大学曾邀请国际著名沉积学家许靖华(Kenneth Jinghua Hsu),共同考察了死海西岸末次冰期湖相剖面(沉积于冰期高水位时期、出露于末次冰消期低水位时期)保存的大型软沉积变形结构(内碎屑角砾层),并肯定其诱因为地震震动。这种事件沉积层在 1995 年被以色列地质学家 Shmuel Marco 和 Amotz Agnon^[100]命名为“mixed layer”,并在 2006 年改称“Intraclast breccia layer”^[101],随后沿用至今。这些变形层位,水平延伸可达数百米至数千米,仅受限于湖岸剖面是否连续出露,可在连续出露的剖面中追踪到。末次冰期湖相沉积序列中的这类事件沉积层,常与同沉积断层共生^[100];而晚全新世(3~0 ka)湖相剖面中的事件沉积层,在时间上可与考古地震事件(3~2 ka)和历史地震事件(2~0 ka)相对应^[102-103],从而证实这类事件沉积为水下震积岩。这些早期(1984~2001 年)开创性的研究,极大的推动了国际湖泊/海洋古地震学的发震。

在 2005 年,Heifetz 等^[104]指出死海湖相序列里保存的各种软沉积变形结构与其他环境(例如,空气和海洋)中出现的由开尔文-亥姆霍兹不稳定性(Kelvin-Helmholtz Instability)触发的变形结构非常相似,暗示它们的形成遵循相似的流体力学机制。他们认为在地震加速度的作用下,死海湖底密度较

小的上部水饱和的松软泥岩层的运动速度快于密度较大的下部泥岩层,二者沿着地震波传输的方向运动,因而产生了位于泥岩层界面的剪切力。基于开尔文-亥姆霍兹不稳定性,Heifetz 等^[104]对这些变形结构进行了线性模拟。

2010 年 Wetzler 等^[105]基于开尔文-亥姆霍兹不稳定性机制以及死海底部水饱和的松软沉积物的物理性质,进行了一系列非线性二维数值模拟;并依据变形程度将软沉积变形结构分成四类:1)线性波浪状变形结构(linear waves);2)不对称巨浪状变形结构(asymmetric billows);3)相互干涉的涡旋状变形结构(coherent vortices);4)涡旋强烈破碎后的内碎屑结构(intraclast breccias)。该工作基于数值模拟定量获取了形成具有不同厚度、不同几何特征的软沉积物变形结构所需的地面加速度(ground acceleration)。这项工作为定量恢复古地震震动强度及震级提供了思路。值得注意的是,这里描述的各种变形结构均不同于常见的负载构造^[106](load structure)。负载构造,由瑞利-泰勒不稳定性(Rayleigh-Taylor Instability)机制驱动,需要沉积层具有上部密度大、下部密度小的反向密度结构。而死海典型的水饱和的松软沉积层的密度随深度增加而增加,具有稳定的正向密度结构,因此,不容易受到瑞利-泰勒不稳定性的影响。

2.1.2 死海湖心 ICDP 5017-1 岩芯保存的震积岩

基于与死海湖岸剖面保存的软沉积变形结构的相似性^[47,100-102,104-105],死海湖心 ICDP 5017-1 岩芯保存的线性波浪状变形结构、不对称巨浪状变形结构、相互干涉的涡旋状变形结构和涡旋强烈破碎后的内碎屑结构被解译为震积岩(图 3)。其中,在前三类沉积结构中,易碎的文石纹层保存完好,可以被追踪,因而表明这些变形结构形成后即被原位保存,未受其他沉积作用的扰动、未经历明显的搬运。否则,任何显著的扰动或搬运过程,都会撕裂或破坏水饱和、且脆弱的亚毫米级文石纹层^[26]。

第四类软沉积变形结构(涡旋强烈破碎后的内碎屑结构)的底部,常由混合的纹层碎屑和相干漩涡残余碎片组成^[70]。大型且完整的这类变形层位,通常由 3 个单元组成:(i)底部未完全破碎的相干涡旋状结构,(ii)中部残留的纹层碎片,(iii)顶部的泥质单元(图 3AP)。这种正粒序结构,指示局部的混合、分选和沉降过程。而混合、分选和沉降过程需要开放的边界条件和流体环境,因而这些过程只能发生于沉积物-湖水界面处,而不能发生在沉积

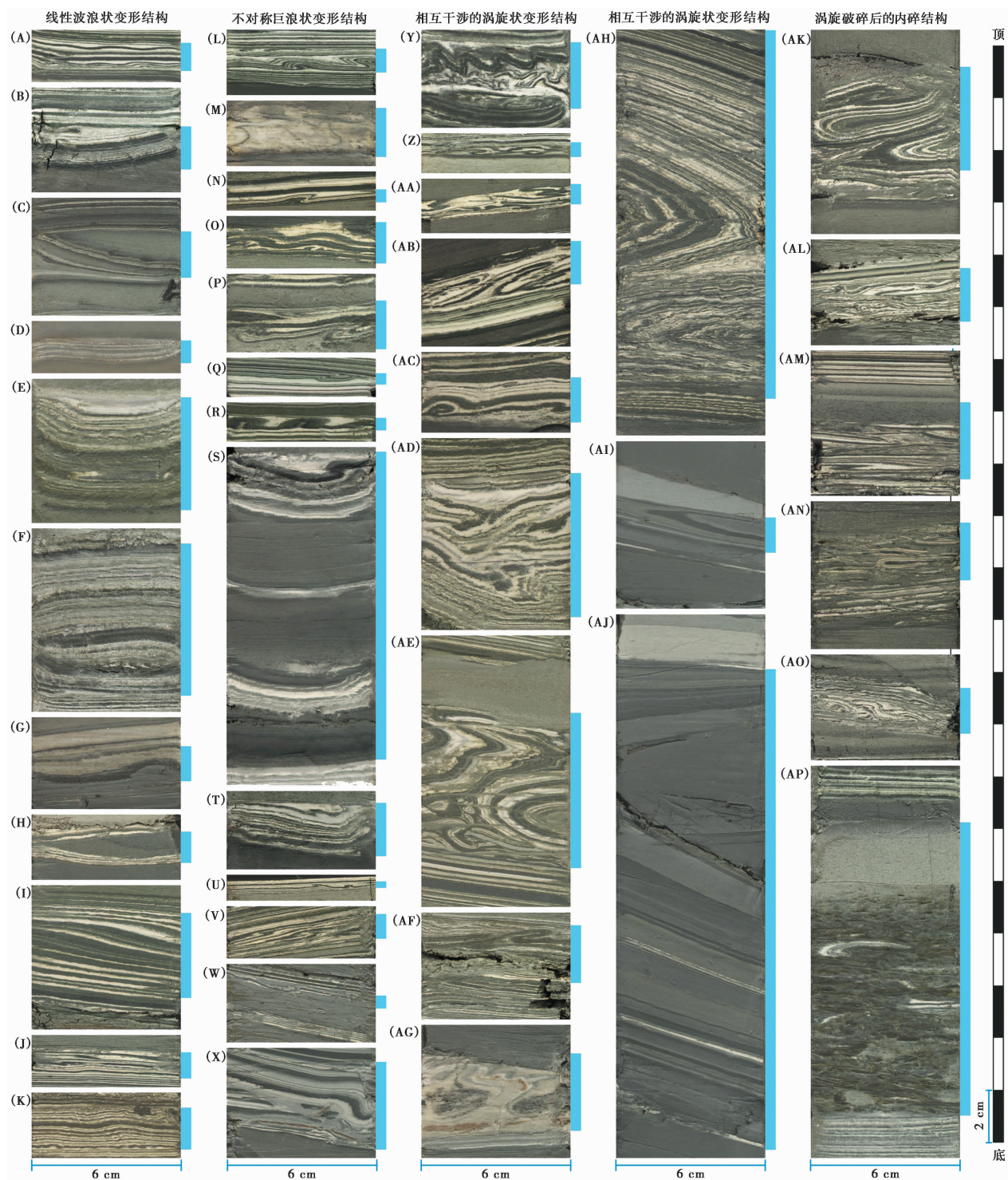


图3 死海 ICDP 5017-1 岩芯保存的震积岩(修改自 Lu 等, 2020^[32])

(A~K) 线性波浪状变形结构; (L~X) 不对称巨浪状变形结构; (Y~AJ) 相互干涉的涡旋状变形结构; (AK~AP) 涡旋破碎后的内碎屑结构
浅蓝色条带指示震积岩层位

Fig. 3 Paleoseismic indicators in the Dead Sea ICDP Core 5017-1(modified from Lu et al. , 2020^[32]). (A~K) Linear waves; (L~X) Asymmetric billows; (Y~AJ) Coherent vortices. (AK~AP) Intraclast breccia layers. The vertical light blue bars indicate the position of seismites

物表面之下(封闭的环境)^[70]。同时, 该类事件沉积层底部没有显著的侵蚀面。因而, 这些沉积层不同于由长距离物质搬运等次生沉积过程形成的纹层碎屑沉积层。

2.2 柴达木盆地(西部)碱山背斜 SG-1b 岩芯保存的震积岩

2.2.1 微断层(micro-faults)

含微断层的沉积层可分为两类: 1) 含单个微断层(single micro-fault)的沉积层(图 4A~4B); 2) 含多个微断层的沉积层(fault-graded bed)(图 4C~4G)。这些微断层的位移从毫米到厘米不等。微断层, 是高应变率引起的脆性变形的结果^[23]。SG-1b 岩芯保存的微断层不是重力作用的结果, 其原因如下: 1) 它们常切穿密度更大的粗粒沉积薄层(图 4A~4B 和 4D~4G); 2) 在较厚的粗粒沉积层(粗粉砂-砂层)的正下方未发现微断层发育; 3) 微断层主要出现在纹层和层状泥岩中(图 4A~4G), 而这种岩性具有稳定的垂向密度结构, 垂直密度差异较小。此外, 这些脆性结构并不局限于岩芯边缘部位, 而常切穿岩芯中心部位; 钻探过程中施加的应力, 并不足以导致这些脆性结构的形成与保存。

此前, 同沉积微断层已在土耳其安纳托利亚^[107]和阿尔卑斯山^[108]的湖泊沉积物中被识别出来, 它们的形成时间与器测或历史地震的发生时间相对应, 因此被解释为震积岩; 此外, 在盆地平静水体沉积序列里发现的包含多个微断层的沉积层, 被认为是由强烈的地震震动产生的震积岩^[23]。我们在 SG-1b 岩芯中观察到的微断层, 与这些已知的变形结构具有高度的相似性, 因此也被认为是古地震的识别标志。

2.2.2 原位软沉积变形(*in situ* soft-sediment deformation)

纹层或薄层间的位移是这类变形结构的主要特征。所有此类结构均出现于纹层和层状泥的岩芯段, 并被纹层和层状泥上覆(图 4H~4L)。这些扰动层的厚度在 3~33 cm 之间。重力失稳, 即瑞利-泰勒不稳定性, 是水下沉积环境中软沉积物变形最常见的驱动力之一^[106, 109]。在 SG-1b 岩芯中, 软沉积物变形层位被层状泥或纹层上覆(图 4H~4L), 且在粗粒沉积层(粗粉砂-砂层)下方未发现此类变形结构。SG-1b 岩芯中的层状泥和纹层具有稳定的垂向密度结构, 垂直密度差异较小, 因而不易发生由反向密度驱动的重力失稳过程。

水下沉积环境中软沉积物变形的另一个常见驱动力是风暴浪^[109]。风暴浪产生的典型变形包括常与风暴沉积(tempestites)有关的重荷模(load-casts)^[110]。在 SG-1b 岩芯中, 识别出的 34 个软沉积变形层位, 均与风暴沉积层无空间关联^[46]; 同时, 所有软沉积变形层位, 均与可指示强烈波浪作用的鲕粒沉积层无空间关联^[46, 96]。因此, 风暴作用不是这些软沉积变形结构的主要触发因素。此外, 我们认为钻探过程中施加的应力, 也不能解释这些变形结构的形成。这是因为人工应力主要作用在岩芯柱的边缘(图 4D), 并不能触发纹层或薄层间的平行位移; 也难以导致位于岩芯中心, 且上、下均受未变形的纹层或薄层限定的变形结构。

这些软沉积变形结构, 与位于构造活跃区(如土耳其安纳托利亚^[107]、智利中南部^[111]、加利福尼亚^[112]和死海^[102])的湖泊沉积物中保存的软沉积变形结构具有高度相似性。上述地区的软沉积物变形结构的形成时间, 可与器测或历史地震(M_w 5.3~9.6)发生的时间相对应, 因而被解释为震积岩^[102, 107, 111~112]。以往的研究表明, 这种由地震引起的软沉积变形发生于水-沉积物界面处^[70, 107, 112]。由于这些变形层位的底部无明显的侵蚀基底, 因而可以排除水下塌等其他重力流过程作为软沉积变形结构的主要触发因素, 也因此, 这些软沉积变形结构是原位形成、保存的。与死海原位软沉积变形结构类似, 我们认为开尔文-亥姆霍兹不稳定性是 SG-1b 岩芯保存的软沉积变形结构的合理驱动机制。因此, 将此类变形结构作为古地震指示标志。

2.2.3 水下塌沉积(slump deposits)

这些塌沉积的显著特征是含有碳酸盐或变形的沉积层(图 4S~4T)。在其底部通常可以观察到显著的侵蚀面或层理滑脱面, 从而将其与上述的原位软沉积物变形结构区分开, 这些塌沉积层的厚度从 3~91 cm 不等。塌沉积包含的碳酸盐使这些层位区别于上覆和下伏的纹层与层状泥, 指示塌沉积的浅水来源; 此外, 塌沉积不含粗砂, 因而不支持碳酸岩源于遥远的湖岸。碳酸岩的最可能来源是碱山背斜顶部海拔较高的区域——那里水深较浅, 利于碳酸盐的形成。

由于碱山背斜顶部缺乏陆源粗颗粒碎屑供应, 沉积速率相对较低且坡度极缓($<1^\circ$), 使得沉积物加载(源于粗颗粒快速堆积)或重力滑动(需要较大的坡度)等非地震触发过程不太可能发生。在这样的环境中, 最可能引发塌沉积的因素是地震震动。即

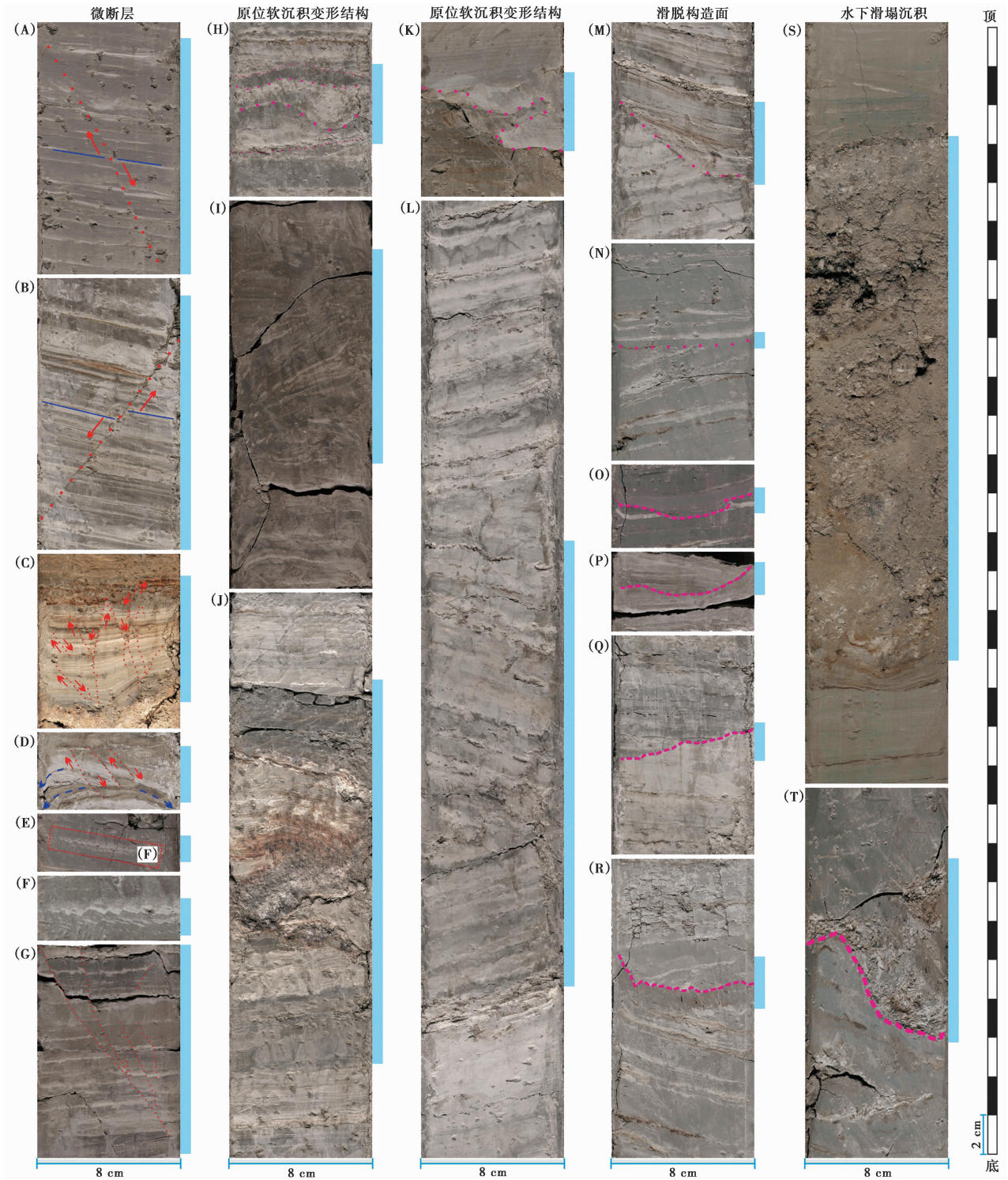


图4 柴达木盆地西部SG-1b岩芯中的古地震指示标志(修改自Lu等, 2021^[46])
 (A~G)微断层;(H~L)原位软沉积变形(褶曲)结构;(M~R)滑脱构造面;(S~T)水下滑塌沉积
 浅蓝色条带指示地震扰动层位

Fig. 4 Paleoseismic indicators in Core SG-1b, western Qaidam Basin(modified from Lu et al. , 2021^[46]).
 (A~G) Micro-faults;(H~L) *In situ* soft-sediment deformations(folded layers);(M~R) Detachment surfaces;
 (S~T) Slump deposits. The vertical light blue bars indicate the position of earthquake-disturbed layers

使在极小的坡度($<1^\circ$)条件下,地震震动也可以触发水下滑塌或沉积物失稳^[113-114]。在阿尔卑斯山脉^[115]和加拿大不列颠哥伦比亚省^[116]的湖泊环境中,曾报道过 5.9~7.5 级的历史地震引发的水下滑塌,这种沉积被解释为震积岩。

2.2.4 滑脱构造面 (Detachment surfaces)

该类结构的特点是尖锐的接触(图 4M~4R)。在此前的研究中,钻孔岩芯中保存的滑脱构造面曾被用于指示区域构造变形^[117-118]和古地震活动^[119]。由于 SG-1b 钻孔位于碱山背斜顶部,我们认为该类滑脱构造面是地震触发的、源于背斜顶部滑塌遗留的痕迹(head scarp)。

3 震积岩序列及其对区域地震-构造活动的启示

3.1 死海盆地基于 ICDP 5017-1 岩芯的震积岩序列

在死海湖心 ICDP 5017-1 岩芯中,我们共识别出 413 个原位软沉积变形层。其中包含 173 个线性波浪状变形层位,101 个不对称巨浪状变形层位,93 个相互干涉的涡旋状变形层位和 46 个涡旋强烈破碎后的内碎屑层位^[32];本文关注于最强烈的变形层位及震级最高的地震事件,基于其中的 93 个相互干涉的涡旋状变形层位和 46 个涡旋强烈破碎后的内碎屑层位,我们建立了死海断裂带中部过去 220 ka 的大地震记录^[32]。

3.1.1 古地震震级约束

为了借助原位变形结构定量恢复地震震动强度,我们更新了由 Wetzler 等^[105]在 2010 年完成的流体动力学模拟。新的模拟结果显示^[32],形成前述线性波浪状变形结构、不对称巨浪状变形结构、相互干涉的涡旋状变形结构和涡旋强烈破碎后的内碎屑结构分别需要 $\geq 0.13\text{ g}$ 、 $\geq 0.18\text{ g}$ 、 $\geq 0.34\text{ g}$ 和 $\geq 0.50\text{ g}$ 的加速度(图 5);此外,所需的加速度也随着变形层位的厚度增加而增加。由于无法确定特定沉积层在地震动时的雷诺数(Reynolds number),我们只能约束具有特定厚度的变形结构所需加速度的下限值。通过同时考虑变形结构的类型和厚度,我们可以获取每个原位软沉积变形层位对应的加速度下限值(表 1)^[32]。利用 Wald 等^[120]提出的峰值地面加速度(Peak Ground Acceleration,简称 PGA)与地震烈度(Modified Mercalli Intensity Scale,简称 MMI)之间的线性关系,可以将加速度 PGA 转换为地震烈度 MMI(表 1)。

考虑到地震能量的耗散,ICDP 5017-1 钻孔附近中等强度地震产生的震动效应可与远处大地震产生的震动效应相似。因此,沿着死海断裂带确定发震位置或范围是实现震级约束的关键所在。由于南-北向延伸的死海断裂带具有相对固定的宽度(约 15 km),我们将 ICDP 5017-1 钻孔向南、北沿着死海断裂带的数百千米范围视为潜在的强震源区(见图 1B);此外,已知 ICDP 5017-1 钻孔与最近的死海底部活动断层间的距离(D)约 5 km。当 $D_{\min} = 5\text{ km}$ 时,基于 3 个已知的死海地区地震能量衰减经验关系^[121-124], $\text{PGA} \geq 0.13\text{ g}$ ($\text{MMI} \geq \text{VI}\frac{1}{2}$) 对应震级下限为 $M_w \geq 5.3$ 。因此,我们将 ICDP 5017-1 岩芯记录的古地震事件震级的下限约束为 $M_w 5.3$ 。

根据 3 个已知的区域地震能量衰减关系^[121-124],ICDP 5017-1 岩芯记录的超强震动强度 $\text{PGA} \geq 0.34\text{ g}$ ($\text{MMI} \geq \text{VIII}$),既可由震中距在 5~30 km 的 6.0~6.9 级地震产生,也可由震中距在 30 km 的 7 级地震产生,或者由震中距远达 150 km 的 8 级地震产生。依据历史及考古地震记录^[63-64],我们估计死海断裂带上合理的最大地震震级为 $M_w 8$ 。这样的地震强度,对应于 300 km 长的沿着主断裂带的地表破裂。因此,我们认为 ICDP 5017-1 岩芯记录的震积岩主要由发生在钻孔位置南、北 150 km 范围内(沿着死海断裂带)的 ≤ 8 级地震造成。在这个滑动缓慢($<5\text{ mm/a}$)的非洲-阿拉伯板块边界上^[48-49],死海断裂带是唯一真正的贡献断层。这是因为转换边缘滑动速率都集中在死海断裂带上,而其他断层要么距离较远,要么滑动速率太低。在死海附近地区,没有其他的断层拥有足够的长度和滑移速率来孕育 7 级地震。

死海断裂带中部过去 2000 年强震的空间分布,为我们约束超强地震震动事件的震级提供了额外的线索。器测^[125]和历史^[63-64,126-127]地震记录显示,在过去 2000 年,所有 $M_w \geq 6$ 地震都发生在距 ICDP 5017-1 钻孔 30 km 之外的地方(见图 1B)。以此作为类比,我们假设在过去 220 ka,绝大多数 $M_w \geq 6$ 地震发生在距 ICDP 5017-1 钻孔 30 km 之外的地方。基于这一假设和区域地震衰减关系^[121-124]可得知,与 $\text{PGA} \geq 0.34\text{ g}$ ($\text{MMI} \geq \text{VIII}$)、 $\text{PGA} \geq 0.50\text{ g}$ ($\text{MMI} \geq \text{VIII}\frac{1}{2}$) 和 $\text{PGA} \geq 0.65\text{ g}$ ($\text{MMI} \geq \text{IX}$) 对应的地震震级分别为 $M_w \geq 7.0$ 、 ≥ 7.3 和 ≥ 7.8 ^[32]。

得益于中东地区研究程度极高的历史地震学^[48,63,127-131]与考古地震学^[42-43,132-134]研究,有关过去 2000 年发生于死海断裂带中部的地震信息较为

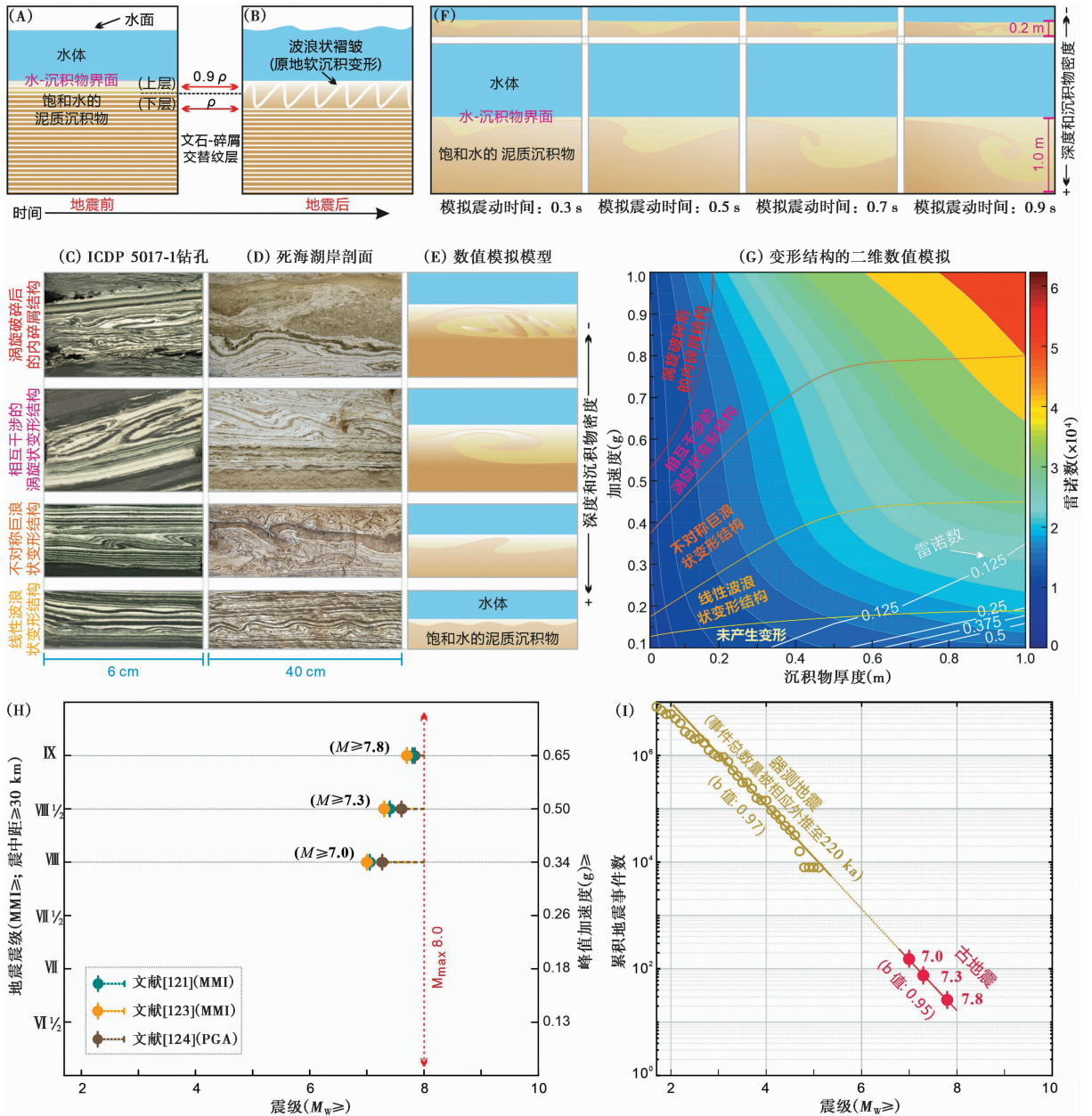


图 5 对死海 ICDP 5017-1 岩芯记录的古地震事件烈度与震级的限定 (修改自 Lu 等, 2020^[32])

(A, B) 图解地震前死海文石-碎屑交替纹层沉积 (A) 与地震后原位软沉积变形结构 (B); (C~E) 死海湖心软沉积变形结构 (C) 与湖岸剖面保存的软沉积变形结构 (D) 的对比, 及其对应的基于开尔文-亥姆霍兹不稳定性机制的数值模拟模型 (E); (F) 图解相同加速度 (1.0 g) 在不同震动时间 (0.3~0.9 s) 下对 0.2 m 和 1.0 m 厚的两个沉积层造成不同程度的变形; (G) 定量估算产生不同厚度的 4 种变形结构所需的加速度; (H) 通过应用 3 个本区地震能量衰减经验公式^[121~124], 并考虑过去 2000 年地震记录, 限定 MMI \geq VIII 事件的震级 (详情请参阅 Lu 等, 2020^[32]); (I) 死海断层中部器测地震^[125] 和 ICDP 5017-1 岩芯记录的过去 220 ka 古地震震级-频率分布

Fig. 5 Intensity and magnitude constraint for paleoearthquakes that recorded in the Dead Sea ICDP Core 5017-1 (modified from Lu et al., 2020^[32]). (A, B) Schematic diagrams showing the aragonite-detritus laminae without seismic disturbance (A), and seismogenic folded layers (B); (C) Typical *in situ* soft-sediment deformation structures from Dead Sea depocenter Core 5017-1; (D) Typical *in situ* soft-sediment deformation structures from Dead Sea onshore outcrops; (E) Schematic diagrams explaining the formation of the four structures based on the Kelvin-Helmholtz Instability mechanism; (F) Comparison of numerical simulation of two horizontal sediments layers at the acceleration of 1.0 g at different simulation time (0.3~0.9 s), for two different layer thicknesses (0.2 m and 1.0 m); (G) Quantitative estimation of the accelerations that are needed to initiate the four *in situ* soft-sediment deformation structures with different thicknesses; (H) Magnitude constraint for strong seismic shaking events (MMI \geq VIII) by applying the three regional empirical attenuation relations^[121~124], taking the past 2000 a earthquake scenario as an analogy for the paleoseismic record; (I) Magnitude-frequency distribution of modern^[125] and paleo-earthquakes on the central Dead Sea Fault during the past 220 ka

表 1 借助流体力学模拟限定死海 ICDP 5017-1 岩芯记录的地震震动强度(修改自 Lu 等, 2020^[32])

Table 1 Constraints on shaking intensities for paleoearthquakes that recorded in the ICDP Core 5017-1 via computational fluid dynamics modeling(modified from Lu et al., 2020^[32])

震积岩类型	厚度 (cm)	加速度 (g)	地震烈度 (MMI)
线性波浪状变形结构	< 59	≥ 0.13	≥ VI½
不对称巨浪状变形结构	< 15	≥ 0.18	> VII
原位褶曲	15~30	0.26~0.34	≥ VII½
相互干涉的涡旋状变形结构	< 13	> 0.34	> VIII
	13~30	0.50~0.65	≥ VIII½
	≥ 30	≥ 0.65	≥ IX
涡旋破碎后的内碎屑结构	0~9	> 0.50	> VIII½
	≥ 9	≥ 0.65	≥ IX

丰富(见图 1B~1C)。我们用已知地震的震级与震中距等信息,检验了我们基于 ICDP 5017-1 岩芯震积岩记录的地震震动强度和区域地震衰减关系的震级限定。结果显示,我们的震级估计值与历史地震震级大小一致,误差为 ±0.3 级^[32],因而表明我们的震级约束是可靠的。

3.1.2 对区域地震-构造活动的启示

由于受到岩芯取心率(<100%)、岩性(如石盐沉积)等因素的影响,ICDP 5017-1 岩芯记录的 $M_w \geq 7$ 事件可能不完整。于是,我们将之前该区域已有的大地震记录与我们的新记录综合集成成为一条 220 ka 的更完整记录^[32](图 6)。已有的大地震记录包括 Begin 等^[135]基于死海西岸露头震积岩建立的 60 ka 的 $M_w \geq 7$ 记录和 Kagan 等^[41,136]基于死海断裂带西部 40 km 处的洞穴沉积建立 185 ka 的 $M_w 8$ 记录(图 6A)。由于 Begin 等^[135]的古地震记录太短,我们将 Kagan 等^[41,136]的古地震记录集成到我们现在的古地震序列中。最终,4 个 $M_w \geq 7$ 历史地震事件(见图 1C)及 8 个基于洞穴震积岩的 $M_w 8$ 地震事件被集成到 220 ka 的古地震序列里(见图 6A)。这 12 个 $M_w \geq 7$ 地震事件,及从 ICDP 5017-1 岩芯中识别的 93 个相互干涉的涡旋状变形层位和 46 个涡旋强烈破碎后的内碎屑层位所代表的 $M_w \geq 7$ 地震事件,一起构成了死海断裂带中部过去 220 ka 连续的大地震记录。

之前的器测、历史和古地震研究表明,在过去 60 ka 期间,死海地区的 Gutenberg-Richter 分布是稳定的,其 b 值为 0.95^[137],与器测地震数据推断的 b 值 0.97 相似^[125](图 51)。集成的 220 ka 的大地震记

录显示 b 值为 0.95^[125],与器测地震 Gutenberg-Richter 分布的 b 值相似(图 51),说明我们对超强地震震动事件的震级限定是合适的、大地震记录是相对完整的。

集成的 220 ka $M_w \geq 7$ 记录揭示地震事件的平均重现时间约为 1400 ± 160 年,事件时间间隔变异系数(coefficient of variation,简称 COV)为 1.43(见图 6A),地震事件时间间隔服从幂律分布^[32](图 6D)。因此,新集成的 220 ka 大地震记录揭示了聚集式的地震复发行及不同断层分支相互作用、聚类活动的模式^[138]。得益于位于盆地沉积中心的位置、极高的沉积速率,ICDP 5017-1 岩芯可能记录了发生于死海沉积中心周边所有分支断层上的强震。当死海断裂带各分支断层的活动(地震)在时间上不协调时,不同断层分支相互作用、聚类活动的模式就会出现;此外,如果在较短的时间间隔内发生地震破裂和不同分支断层间的应力转移,随后出现长时间的宁静期,也会导致不同断层分支聚类活动模式的出现。死海断裂带作为几何形状复杂、滑动缓慢的板块边界的代表,具有不同于几何形状相对简单、滑动快速的走滑断裂带(如新西兰的阿尔卑斯断裂带^[45])特有的准周期性地震复发模式。

3.2 柴达木盆地(西部)基于 SG-1b 岩芯的震积岩序列

在 SG-1b 岩芯上部 260 m(3.6~1.6 Ma),我们识别出 79 层含微断层的沉积层,34 个原位软沉积变形层位,41 个滑塌沉积层和 10 个滑脱构造面;基于 SG-1b 岩芯上部 260 m 保存的 164 个震积岩层位,我们建立了一个覆盖 3.6~1.6 Ma 的震积岩序列^[46]。该震积岩序列在 3.6~2.7 Ma 时段内相对较为连续,由发生于 3.6~3.5 Ma、3.4~3.2 Ma、3.15~3.10 Ma、3.0~2.9 Ma 和 2.80~2.75 Ma 的这 5 个地震集合组成,包含 126 个事件。

3.2.1 古地震主要源区及震级限定

柴达木盆地西部的一级断裂带包括阿尔金断裂带和昆仑断裂带。全新世探槽古地震记录揭示,距碱山背斜 SG-1b 钻孔最近的阿尔金断裂带索尔库里段^[36]和阿克塞段^[139](见图 1B和图 7C)的强震具有准周期性的复发模式,其平均复现时间分别为 0.6 ka(在 6~0 ka 期间)和 1.4 ka(在 8~0 ka 期间)。以往的研究也表明,在过去数百万年的时间里,阿尔金断裂带具有相对稳定的变形速率,约为 9 mm/a^[140],与 GPS 测量结果一致^[141-142]。因而,

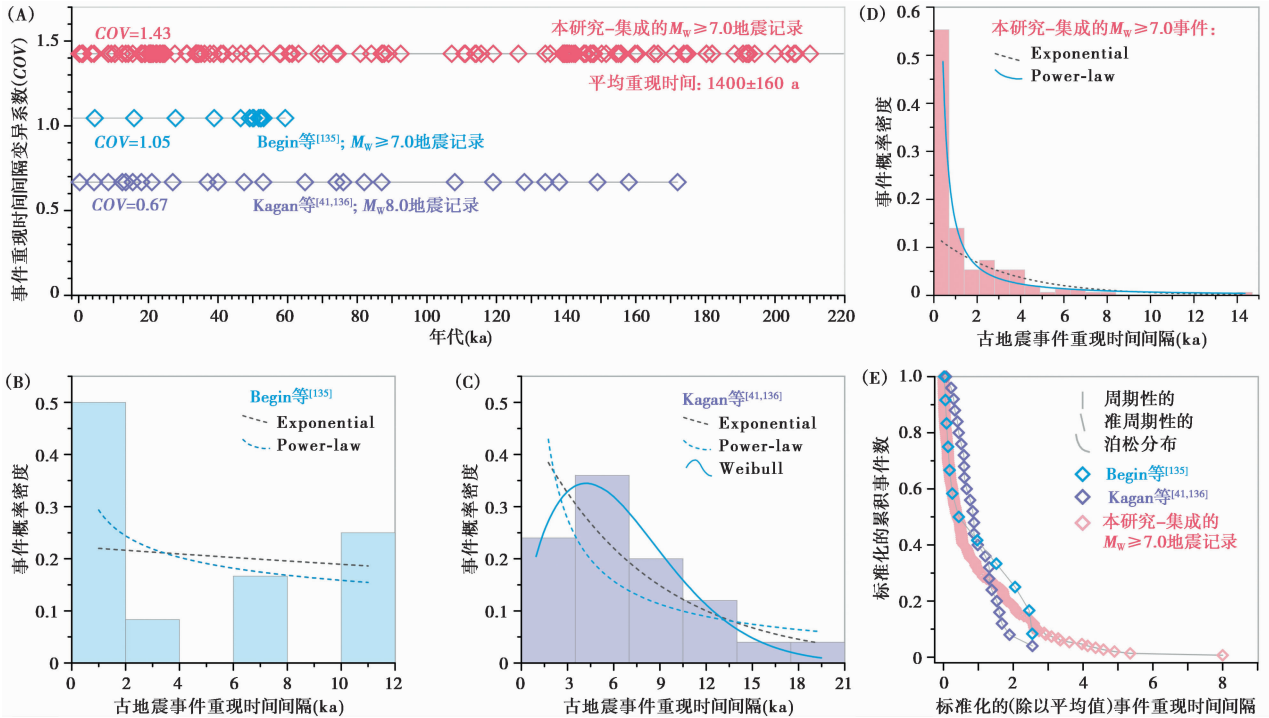


图6 死海过去 220 ka 地震记录揭示的大地震 ($M_w \geq 7.0$) 复发模式 (修改自 Lu 等, 2020^[32])

(A) 死海地区 3 个不同时间尺度、基于不同地震标志的大地震记录对比; (B) 基于死海西部 Peratzim 湖岸剖面 (图 1B) 建立的 $M_w \geq 7.0$ 地震记录及其事件重现时间间隔分布^[135]; (C) 基于死海西北部 Soreq 和 Har-Tuv 洞穴沉积 (图 1B) 建立的 $M_w 8.0$ 地震记录及其事件重现时间间隔分布^[41,136]; (D) 本研究重建的大地震 ($M_w \geq 7.0$) 记录及事件重现时间间隔分布; (E) 基于 3 个大地震记录的均一化的事件重现时间间隔分布的对比

Fig. 6 Recurrence pattern of large earthquakes ($M_w \geq 7.0$) on the slow-slipping Dead Sea Fault during the past 220 ka (modified from Lu et al., 2020^[32]). (A) Comparison of different temporal distributions of large earthquakes on the central Dead Sea Fault Zone derived from three different geological records; (B) Histograms for recurrence times of $M_w \geq 7.0$ events in the paleoseismic record of Begin et al. ^[135]; (C) Histograms for recurrence times of ca. $M_w 8.0$ events in the paleoseismic record of Kagan et al. ^[41,136]; (D) Histograms for recurrence times in the integrated 220 ka-long $M_w \geq 7.0$ record (this study); (E) Normalized recurrence data for the three datasets for comparison

SG-1b 钻孔附近的阿尔金断裂带在过去数百万年间很可能具有准周期性的破裂行为; 此外, 前人基于河流阶地的古地震学研究表明, 距离碱山背斜 SG-1b 钻孔最近的东昆仑断裂带西段 (距 SG-1b 钻孔 ≥ 300 km) 在 8~2 ka 期间 8 级地震的平均复现时间约为 0.9 ka^[143]。如果阿尔金断裂带和昆仑断裂带是 SG-1b 岩芯记录的古地震的主要来源, 那么 SG-1b 岩芯记录的古地震事件的平均重现间隔必将远远小于 0.6 ka。

然而, SG-1b 岩芯记录的发生于 3.6~2.7 Ma 的 5 个古地震集合的最小平均重现间隔为 4.0 ka。此外, SG-1b 震积岩序列具有极高的 COV 值 (1.3)^[46], 表明该钻孔位置主要受碱山背斜周围几何形状复杂的逆冲系统的影响。这些特征表明, 邻近的局部构造 (褶皱、背斜) 而非远端的阿尔金断裂

带或昆仑断裂带才是古地震的主要源区。这些褶皱、背斜发育在湖底浅层逆冲构造上, 其轴向长度为 20~50 km, 理论上可孕育中等强度地震 ($M_w \geq 5$)。以往的湖泊/海洋古地震学研究表明^[101,107-108,111-112,115-116,144-146], 震中距 < 60 km 的中等强度地震足以诱发各种震积岩 (见图 7A)。因此, SG-1b 震积岩序列的高 COV 值和很长的重现时间间隔均值 (6.8 ± 0.8 ka, 见图 7B), 指示柴达木盆地西部地区的碱山背斜及其周围的褶皱和逆冲构造是古地震的主要源区 (图 7C)。

3.2.2 对区域地震-构造活动的启示

SG-1b 岩芯记录了 3.6~2.7 Ma 期间的 5 个震积岩集合 (图 8), 这种地震集聚模式表明^[46], 柴达木盆地逆冲断层系统吸纳的构造应力随时间变化而不同, 揭示了该地区具有幕式褶皱-冲断变形特征。

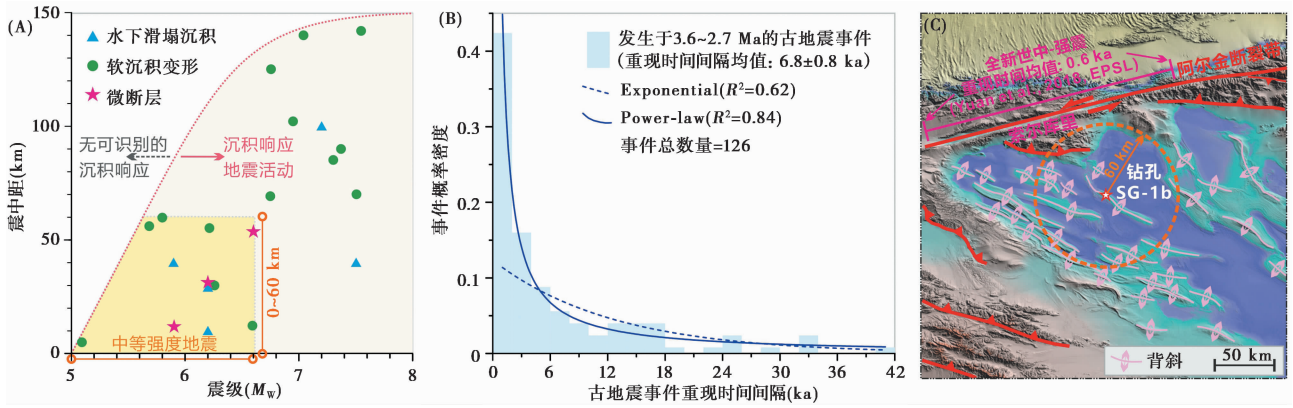


图 7 对柴达木盆地西部 SG-1b 岩芯记录的古地震事件震级的约束 (修改自 Lu 等, 2021^[46])

(A) 基于全球范围内研究案例的震级-震中距图解, 展示微断层^[107-108]、水下原位软沉积变形^[101,107,111-112]和 水下滑塌沉积^[115-116,144-146]等响应地震活动对应的阈值; 左下角黄色区域指示震中距 ≤ 60 km 的中等强度地震引起的事件沉积效应;

(B) 3.6~2.7 Ma 期间古地震事件重现时间间隔的分布及其指数与幂律分布的拟合; (C) SG-1b 钻孔附近的背斜分布^[81]

Fig. 7 Magnitude constraint for paleoearthquakes that recorded in Core SG-1b from the western Qaidam Basin (modified from Lu et al. , 2021^[46]). (A) Instrumental and historical earthquake magnitude vs. epicentral distance plot based on literature to show thresholds for micro-faults^[107-108], soft-sediment deformation^[101,107,111-112] and slumps^[115-116,144-146] in subaqueous environments in different regions. The yellow-colored area highlights the seismic effects of moderate earthquakes with epicentral distance ≤ 60 km; (B) Histograms for recurrence times of events during 3.6 ~ 2.7 Ma. Exponential and power-law distributions are plotted for comparison; (C) Anticlines surrounding Core SG-1b^[81]

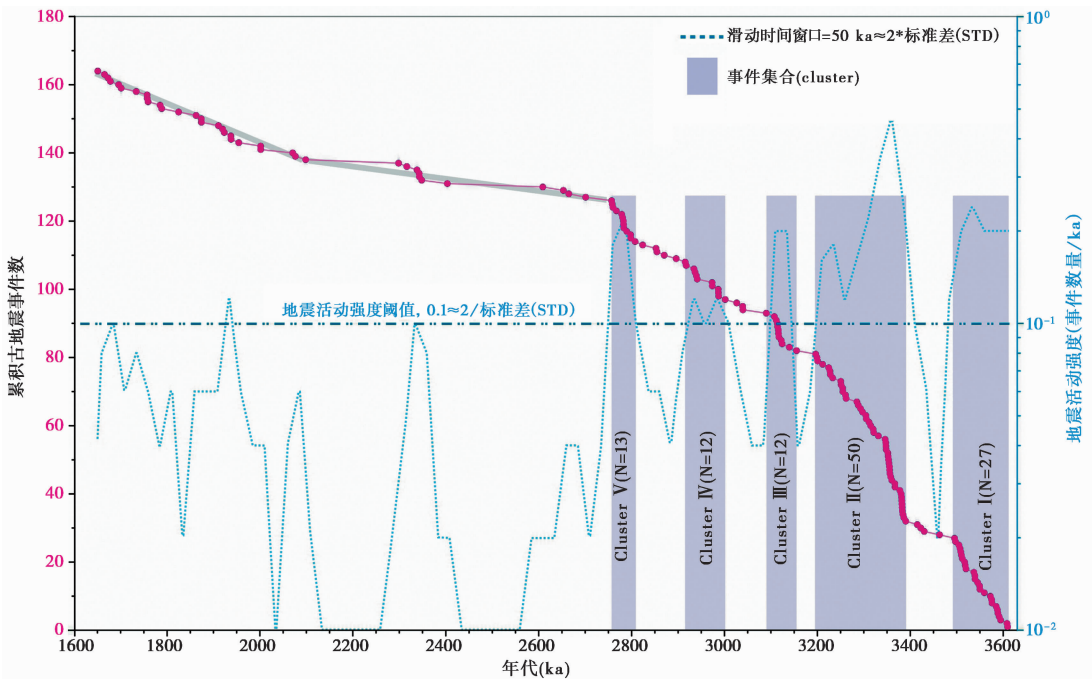


图 8 柴达木盆地西部 SG-1b 岩芯记录的 3.6~1.6 Ma 期间的震积岩序列 (修改自 Lu 等, 2021^[46])

Fig. 8 Distribution of seismites in Core SG-1b from the western Qaidam Basin during 3.6 ~ 1.6 Ma (modified from Lu et al. , 2021^[46])

然而, 以往的研究表明, 该地区的阿尔金断裂带在过去几百万年间很可能具有准周期性的破裂行为^[36,139-140]。因此, 我们提出在地震聚集发生期间, 区域形变主要集中于盆地内的褶皱-逆冲断层

体系; 而在地震平静期, 区域形变主要沿着阿尔金与昆仑走滑断裂带分布。这两种体系在地震聚集发生期及地震平静期可能吸收了相同量的由印度-亚欧板块碰撞引起的远程构造载荷。

4 结语、问题与展望

基于死海湖心 ICDP 5017-1 岩芯震积岩序列集成的 220 ka 大地震 ($M_w \geq 7$) 记录, 是死海断裂带上最长、最完整、最具代表性的古地震记录, 也是全球大型断裂带上最长的连续大地震记录。不同于快速滑动和几何形状相对简单的走滑断裂带特有的准周期性强震复发模式, 死海 220 ka 大地震记录揭示了缓慢滑动、几何形状复杂的死海断裂带具有非周期性的强震复发行和不同分支断层聚类活动的模式。

基于柴达木盆地 SG-1b 岩芯的震积岩序列, 记录了发生于 3.6~2.7 Ma 期间的 5 个地震集合, 揭示了与强烈区域变形有关的幕式逆冲过程。在地震聚集发生期间, 区域形变主要集中于盆地内的褶皱-逆冲断层体系; 而在地震平静期, 区域形变主要沿着阿尔金与昆仑走滑断裂带分布。这两种体系在地震聚集发生期及地震平静期可能吸收了相同量的由印度-亚欧板块碰撞引起的远程构造载荷。

建立长尺度震积岩序列的关键在于解决以下几个方面的问题: 第一, 合适的研究区域的选择。位于构造活跃区、邻近活动断裂带的水下沉积具有更低的响应新构造活动的阈值; 第二, 合适材料的获取。需要获得沉积连续、沉积速率较高、时间跨度较长的水下沉积序列; 第三, 古地震标志的确定。需要通过精细的、高分辨率的沉积学分析, 结合具体的地质环境, 基于对水下沉积过程的充分理解, 论证地震震动而非其他非地震因素是目标事件沉积的最合理的触发因素。

不同于盆地沉积序列的岩性、粒度与沉积速率等混合性沉积学指标, 震积岩是独立于气候因素的沉积学证据, 因而能可靠的指示区域新构造活动。此外, 基于水下沉积序列获取的长尺度震积岩序列所包含的古地震事件数量, 通常会远多于该沉积序列年龄控制点(如古地磁定年或铀-钍定年)的数量。因而, 与基于相同水下沉积序列建立的岩性、沉积速率等常规指标序列相比, 震积岩序列具有更高的时间分辨率, 能更精细的反映区域新构造活动随时间的变化过程。此类研究, 将古地震事件、古地震复发模式与构造尺度上的区域形变相联系, 为理解区域构造形变提供了一个新视角, 可以拓展沉积学和古地震学理解区域构造形变问题的能力。

致谢: 本文是受石许华、张会平和王伟涛教授

邀请(“新构造与地貌”专辑), 并在本文作者及其他合作者前期工作基础上撰写的。本文第一作者卢银博士获 2022 年欧洲地球科学联合会(EGU)地层学、沉积学、古生物学领域“青年科学家奖”(Stratigraphy, Sedimentology and Palaeontology Division Outstanding Early Career Scientist Award), 本文是对主要获奖内容的总结; 更详细、全面的研究细节请参阅本文文献[26]、[32]、[46]和[70~71]。感谢前期合作者们对本文研究成果的贡献。感谢两位审稿人及编辑部杨美芳老师提供的宝贵的修改建议。

参考文献(References):

- [1] Stewart I. Neotectonics[M]// Selley R C, Cocks L R M, Plimer I R. Encyclopedia of Geology. Oxford: Elsevier, 2005: 425-428.
- [2] 张培震. 中国大陆岩石圈最新构造变动与地震灾害[J]. 第四纪研究, 1999, (5): 404-413.
Zhang Peizhen. Late Quaternary tectonic deformation and earthquake hazard in continental China[J]. Quaternary Sciences, 1999, (5): 404-413.
- [3] 张培震, 邓起东, 张竹琪, 等. 中国大陆的活动断裂, 地震灾害及其动力过程[J]. 中国科学: 地球科学, 2013, 43(10): 1607-1620.
Zhang Peizhen, Deng Qidong, Zhang Zhuqi, et al. Active faults, earthquake hazards and associated geodynamic processes in continental China[J]. Science China: Earth Sciences, 2013, 43(10): 1607-1620.
- [4] Wu Z, Hu M. Neotectonics, active tectonics and earthquake geology: Terminology, applications and advances[J]. Journal of Geodynamics, 2019, 127: 1-15. doi:10.1016/j.jog.2019.01.007.
- [5] Molnar P, Anderson R S, Anderson S P. Tectonics, fracturing of rock, and erosion[J]. Journal of Geophysical Research: Earth Surface, 2007, 112(F3). doi:10.1029/2005JF000433.
- [6] Larsen I J, Montgomery D R. Landslide erosion coupled to tectonics and river incision[J]. Nature Geoscience, 2012, 5(7): 468-473.
- [7] Dadson S J, Hovius N, Chen H, et al. Links between erosion, runoff variability and seismicity in the Taiwan orogen[J]. Nature, 2003, 426(6967): 648-651.
- [8] Hay W W, Shaw C A, Wold C N. Mass-balanced paleogeographic reconstructions[J]. Geologische Rundschau, 1989, 78(1): 207-242.
- [9] Blackstone Jr D. Late Cretaceous and Cenozoic history of Laramie Basin region, southeast Wyoming[J]. Geological Society of America Memoir, 1975, 144(1975): 249-279.
- [10] Liu T, Ding M, Derbyshire E. Gravel deposits on the margins of the Qinghai-Xizang Plateau, and their environmental significance [J]. Palaeogeography, Palaeoclimatology, Palaeoecology, 1996, 120(1-2): 159-170.
- [11] Zheng H, Powell C M, An Z, et al. Pliocene uplift of the northern Tibetan Plateau[J]. Geology, 2000, 28(8): 715-718.
- [12] Pares J M, Wagoner der Voo R, Downs W R, et al. Northeastward

- growth and uplift of the Tibetan Plateau: Magnetostratigraphic insights from the Guide Basin[J]. *Journal of Geophysical Research: Solid Earth*, 2003, 108(B1). doi:10.1029/2001JB001349.
- [13] Fang X, Yan M, Wagoner der Voo R, et al. Late Cenozoic deformation and uplift of the NE Tibetan Plateau: Evidence from high-resolution magnetostratigraphy of the Guide Basin, Qinghai Province, China[J]. *Geological Society of America Bulletin*, 2005, 117(9):1208–1225.
- [14] Wang P, Scherler D, Liu-Zeng J, et al. Tectonic control of Yarlung Tsangpo Gorge revealed by a buried canyon in southern Tibet[J]. *Science*, 2014, 346(6212):978–981.
- [15] 李吉均, 文世宣, 张青松, 等. 青藏高原隆起的时代、幅度和形式的探讨[J]. *中国科学(D辑)*, 1979, 9(6):608–616.
Li Jijun, Wen Shixuan, Zhang Qingsong, et al. A discussion on the period, amplitude and type of the uplift of the Tibetan Plateau[J]. *Science in China(Series D)*, 1979, 9(6):608–616.
- [16] 于祥江, 郭召杰, 张道伟, 等. 第四纪悸动: 来自柴达木盆地构造增强的证据及其对多圈层的响应[J]. *第四纪研究*, 2018, 38(1):39–53.
Yu Xiangjiang, Guo Zhaojie, Zhang Daowei, et al. Quaternary shaking: Evidences of tectonic intensification from the Qaidam Basin and its influence on multi-spherical interaction[J]. *Quaternary Sciences*, 2018, 38(1):39–53.
- [17] Yu X, Guo Z. The role of base level, watershed attribute and sediment accumulation in the landscape and tectonic evolution of the Circum-Tibetan Plateau Basin and Orogen System[J]. *Journal of Asian Earth Sciences*, 2019, 186:104053. doi:10.1016/j.jseaes.2019.104053.
- [18] Molnar P, England P. Late Cenozoic uplift of mountain ranges and global climate change: Chicken or egg? [J]. *Nature*, 1990, 346(6279):29–34.
- [19] Zhang P Z, Molnar P, Downs W R. Increased sedimentation rates and grain sizes 2–4 Myr ago due to the influence of climate change on erosion rates[J]. *Nature*, 2001, 410(6831):891–897.
- [20] Molnar P. Late Cenozoic increase in accumulation rates of terrestrial sediment; How might climate change have affected erosion rates? [J]. *Annual Review of Earth and Planetary Sciences*, 2004, 32:67–89. doi:10.1146/annurev.earth.32.091003.143456.
- [21] Molnar P. Climate change, flooding in arid environments, and erosion rates[J]. *Geology*, 2001, 29(12):1071–1074.
- [22] Seilacher A. Sedimentary structures tentatively attributed to seismic events[J]. *Marine Geology*, 1984, 55(1–2):1–12.
- [23] Seilacher A. Fault-graded beds interpreted as seismites[J]. *Sedimentology*, 1969, 13(1–2):155–159.
- [24] McCalpin J P, Nelson A R. Chapter 1: Introduction to paleoseismology [M] // McCalpin J P. *Paleoseismology*. Burlington: Elsevier, 2009: 1–27.
- [25] 乔秀夫, 李海兵, 苏德辰, 等. 软沉积物变形构造——地震与古地震记录[M]. 北京: 地质出版社, 2017:1–263.
Qiao Xiufu, Li Haibing, Su Dechen, et al. Soft Sediment Deformation—Earthquake and Paleoseismic Record[M]. Beijing: Geological Publishing House, 2017:1–263.
- [26] Lu Y, Waldmann N, Ian Alsop G, et al. Interpreting soft sediment deformation and mass transport deposits as seismites in the Dead Sea depocenter[J]. *Journal of Geophysical Research: Solid Earth*, 2017, 122:8305–8325. doi:10.1002/2017JB014342.
- [27] 乔秀夫, 李海兵. 沉积物的地震及古地震效应[J]. *古地理学报*, 2009, 11(6):593–610.
Qiao Xiufu, Li Haibing. Effect of earthquake and ancient earthquake on sediments[J]. *Journal of Paleogeography*, 2009, 11(6):593–610.
- [28] Chen A, Zhong Y, Ogg J G, et al. Traces of the Triassic collision between the North and South China blocks in the form of seismites and other event layers[J]. *Journal of Geodynamics*, 2020, 136:101720. doi:10.1016/j.jog.2020.101720.
- [29] 师骏, 黄伟康, 尚江伟, 等. 塔里木盆地西北缘新元古代震积岩的发现及其地质意义[J]. *地质科学*, 2021, 56(3):758–769.
Shi Jun, Huang Weikang, Shang Jiangwei, et al. Discovery of Neoproterozoic seismites in the northwestern margin of the Tarim Basin and its geological significance[J]. *Chinese Journal of Geology*, 2021, 56(3):758–769.
- [30] 田洪水, Wagoner Loon A J, 王华林, 等. 大盛群中的震积岩: 郯庐断裂带强构造与地震活动新证据[J]. *中国科学: 地球科学*, 2015, 46(1):79–96.
Tian Hongshui, Wagoner Loon A J, Wang Hualin, et al. 2016. Seismites in the Dasheng Group: New evidences of strong tectonic and earthquake activities of the Tanlu Fault Zone[J]. *Science China: Earth Sciences*, 2016, 46(1):79–96.
- [31] Goldfinger C, Morey A E, Nelson C H, et al. Rupture lengths and temporal history of significant earthquakes on the offshore and north coast segments of the Northern San Andreas Fault based on turbidite stratigraphy[J]. *Earth and Planetary Science Letters*, 2007, 254(1–2):9–27.
- [32] Lu Y, Wetzler N, Waldmann N, et al. A 220,000-year-long continuous large earthquake record on a slow-slipping plate boundary[J]. *Science Advances*, 2020, 6(48). doi:10.1126/sciadv.aba4170.
- [33] Strasser M, Anselmetti F S, Fäh D, et al. Magnitudes and source areas of large prehistoric northern Alpine earthquakes revealed by slope failures in lakes[J]. *Geology*, 2006, 34(12):1005–1008.
- [34] Moernaut J, Wagoner Daele M, Fontijn K, et al. Larger earthquakes recur more periodically: New insights in the megathrust earthquake cycle from lacustrine turbidite records in south-central Chile[J]. *Earth and Planetary Science Letters*, 2018, 481:9–19. doi:10.1016/j.epsl.2017.10.016.
- [35] Sieh K E. Slip along the San Andreas fault associated with the great 1857 earthquake[J]. *Bulletin of the Seismological Society of America*, 1978, 68(5):1421–1448.
- [36] Yuan Z, Liu-Zeng J, Wang W, et al. A 6000-year-long paleoseismologic record of earthquakes along the Xorkoli section of the Altyn Tagh Fault, China[J]. *Earth and Planetary Science Letters*, 2018, 497:193–203. doi:10.1016/j.epsl.2018.06.008.
- [37] Scharer K M, Weldon R J, Fumal T E, et al. Paleoequakes on the southern San Andreas Fault, Wrightwood, California, 3000

- to 1500 B. C. : A new method for evaluating paleoseismic evidence and earthquake horizons[J]. *Bulletin of the Seismological Society of America*, 2007, 97(4):1054–1093.
- [38] Jacoby G C, Sheppard P R, Sieh K E. Irregular recurrence of large earthquakes along the San Andreas fault: Evidence from trees[J]. *Science*, 1988, 241(4862):196–199.
- [39] Fan J, Wei X, Shi W, et al. Response of tree rings to earthquakes during the past 350 years at Jiuzhaigou in the eastern Tibet[J]. *Science of the Total Environment*, 2020, 731:138714. doi:10.1016/j.scitotenv.2020.138714.
- [40] Szczygieł J, Sobczyk A, Hercman H, et al. Damaged speleothems and collapsed karst chambers indicate paleoseismicity of the NE Bohemian Massif (Niedźwiedzia Cave, Poland) [J]. *Tectonics*, 2021, 40:e2020TC006459. doi:10.1029/2020TC006459.
- [41] Kagan E J, Agnon A, Bar-Matthews M, et al. Dating large infrequent earthquakes by damaged cave deposits[J]. *Geology*, 2005, 33(4):261–264.
- [42] Ellenblum R, Marco S, Kool R, et al. Archaeological record of earthquake ruptures in Tell Ateret, the Dead Sea Fault[J]. *Tectonics*, 2015, 34(10):2105–2117.
- [43] Marco S, Hartal M, Hazan N, et al. Archaeology, history, and geology of the AD 749 earthquake, Dead Sea transform[J]. *Geology*, 2003, 31(8):665–668.
- [44] 刘静, 袁兆德, 徐岳仁, 等. 古地震学: 活动断裂震复发规律的研究[J]. *地学前缘*, 2021, 28(2):211–231.
Liu Jing, Yuan Zhaode, Xu Yueren, et al. Paleoseismic investigation of the recurrence behavior of large earthquakes on active faults[J]. *Earth Science Frontiers*, 2021, 28(2):211–231.
- [45] Berryman K R, Cochran U A, Clark K J, et al. Major earthquakes occur regularly on an isolated plate boundary fault[J]. *Science*, 2012, 336(6089):1690–1693.
- [46] Lu Y, Marco S, Wetzler N, et al. A paleoseismic record spanning 2-Myr reveals episodic Late Pliocene deformation in the western Qaidam Basin, NE Tibet[J]. *Geophysical Research Letters*, 2021, 48(5):e2020GL090530. doi:10.1029/2020GL090530.
- [47] Marco S, Stein M, Agnon A, et al. Long-term earthquake clustering: A 50,000 years paleoseismic record in the Dead Sea Graben[J]. *Journal of Geophysical Research*, 1996, 101(B3):6179–6192.
- [48] Marco S, Klinger Y. Review of on-fault palaeoseismic studies along the Dead Sea Fault [M] // Garfunkel Z, Ben-Avraham Z, Kagan E. *Dead Sea Transform Fault System: Reviews*. Dordrecht: Springer, 2014:183–205.
- [49] Ben-Avraham Z, Garfunkel Z, Lazar M. Geology and evolution of the southern Dead Sea Fault with emphasis on subsurface structure[J]. *Annual Review of Earth and Planetary Sciences*, 2008, 36:357–387. doi:10.1146/annurev.earth.36.031207.124201.
- [50] Weldon R J, Fumal T E, Biasi G P, et al. Past and future earthquakes on the San Andreas Fault[J]. *Science*, 2005, 308(5724):966–967.
- [51] Howarth J D, Barth N C, Fitzsimons S J, et al. Spatiotemporal clustering of great earthquakes on a transform fault controlled by geometry[J]. *Nature Geoscience*, 2021, 14(5):314–320.
- [52] Cochran U A, Clark K J, Howarth J D, et al. A plate boundary earthquake record from a wetland adjacent to the Alpine fault in New Zealand refines hazard estimates[J]. *Earth and Planetary Science Letters*, 2017, 464:175–188. doi:10.1016/j.epsl.2017.02.026.
- [53] Cowgill E, Gold R D, Xuanhua C, et al. Low Quaternary slip rate reconciles geodetic and geologic rates along the Altyn Tagh Fault, northwestern Tibet[J]. *Geology*, 2009, 37(7):647–650.
- [54] Elliott A J, Oskin M E, Liu-Zeng J, et al. Rupture termination at restraining bends: The last great earthquake on the Altyn Tagh Fault[J]. *Geophysical Research Letters*, 2015, 42(7):2164–2170.
- [55] Neev D, Emery K O. The Dead Sea, depositional processes and environments of evaporites. [J]. *Geological Survey of Israel Bulletin*, 1967, 41(1967):1–147.
- [56] Stein M. The sedimentary and geochemical record of Neogene-Quaternary water bodies in the Dead Sea Basin—Inferences for the regional paleoclimatic history[J]. *Journal of Paleolimnology*, 2001, 26(3):271–282.
- [57] Begin Z B, Ehrlich A, Nathan Y. Lake Lisan the Pleistocene precursor of the Dead Sea[J]. *Geological Survey of Israel Bulletin*, 1974, 63(1974):1–30.
- [58] Bartov Y, Stein M, Enzel Y, et al. Lake levels and sequence stratigraphy of Lake Lisan, the Late Pleistocene Precursor of the Dead Sea[J]. *Quaternary Research*, 2002, 57(1):9–21.
- [59] Langgut D, Neumann F H, Stein M, et al. Dead Sea pollen record and history of human activity in the Judean Highlands (Israel) from the Intermediate Bronze into the Iron Ages (~2500–500 BCE) [J]. *Palynology*, 2014, 38(2):280–302.
- [60] Enzel Y, Bookman R, Sharon D, et al. Late Holocene climates of the Near East deduced from Dead Sea level variations and modern regional winter rainfall[J]. *Quaternary Research*, 2003, 60(3):263–273.
- [61] Bartov Y, Agnon A, Enzel Y, et al. Late Quaternary faulting and subsidence in the central Dead Sea basin[J]. *Israel Journal of Earth Sciences*, 2006, 55(1):17–31.
- [62] Levi T, Bausch D, Katz O, et al. Insights from Hazus loss estimations in Israel for Dead Sea transform earthquakes[J]. *Natural Hazards*, 2014, 75(1):365–388.
- [63] Agnon A. Pre-instrumental earthquakes along the Dead Sea Rift [M] // Garfunkel Z, Ben-Avraham Z, Kagan E. *Dead Sea Transform Fault System: Reviews*. Dordrecht: Springer, 2014:207–261.
- [64] Lefevre M, Klinger Y, Al-Qaryouti M, et al. Slip deficit and temporal clustering along the Dead Sea Fault from paleoseismological investigations[J]. *Scientific Reports*, 2018, 8(1). doi:10.1038/s41598-41018-22627-41599.
- [65] Kitagawa H, Stein M, Goldstein S L, et al. Radiocarbon chronology of the DSDDP core at the deepest floor of the Dead Sea[J]. *Radiocarbon*, 2017, 59(2):383–394.
- [66] Goldstein S L, Kiro Y, Torfstein A, et al. Revised chronology of the

- ICDP Dead Sea deep drill core relates drier-wetter-drier climate cycles to insolation over the past 220 kyr[J]. *Quaternary Science Reviews*, 2020, 244:106460. doi:10.1016/j.quascirev.2020.106460.
- [67] Stein M, Ben-Avraham Z, Goldstein S, et al. Deep drilling at the Dead Sea[J]. *Scientific Drilling*, 2011, (11):46-47.
- [68] Neugebauer I, Brauer A, Schwab M J, et al. Lithology of the long sediment record recovered by the ICDP Dead Sea Deep Drilling Project(DSDDP)[J]. *Quaternary Science Reviews*, 2014, 102:149-165. doi:10.1016/j.quascirev.2014.08.013.
- [69] Torfstein A, Goldstein S L, Kushnir Y, et al. Dead Sea drawdown and monsoonal impacts in the Levant during the last interglacial[J]. *Earth and Planetary Science Letters*, 2015, 412:235-244. doi:10.1016/j.epsl.2014.12.013.
- [70] Lu Y, Moernaut J, Bookman R, et al. A new approach to constrain the seismic origin for prehistoric turbidites as applied to the Dead Sea Basin[J]. *Geophysical Research Letters*, 2021, 48(3). doi:10.1029/2020GL090947.
- [71] Lu Y, Moernaut J, Waldmann N, et al. Orbital-and millennial-scale changes in lake-levels facilitate earthquake-triggered mass failures in the Dead Sea Basin[J]. *Geophysical Research Letters*, 2021, 48(14). doi:10.1029/2021GL093391.
- [72] Kiro Y, Goldstein S L, Lazar B, et al. Environmental implications of salt facies in the Dead Sea[J]. *Geological Society of America Bulletin*, 2016, 128:824-841. doi:10.1130/b31357.1.
- [73] Ben Dor Y, Armon M, Ahlborn M, et al. Changing flood frequencies under opposing Late Pleistocene eastern Mediterranean climates[J]. *Scientific Reports*, 2018, 8(1):8445. doi:10.1038/s41598-018-25969-6.
- [74] Lu Y, Bookman R, Waldmann N, et al. A 45 kyr laminae record from the Dead Sea: Implications for basin erosion and floods recurrence[J]. *Quaternary Science Reviews*, 2020, 229:106143. doi:10.1016/j.quascirev.2019.106143.
- [75] Lu Y, Waldmann N, Nadel D, et al. Increased sedimentation following the Neolithic Revolution in the Southern Levant[J]. *Global and Planetary Change*, 2017, 152:199-208. doi:10.1016/j.gloplacha.2017.04.003.
- [76] Katz A, Kolodny Y, Nissenbaum A. The geochemical evolution of the Pleistocene Lake Lisan—Dead Sea system[J]. *Geochimica et Cosmochimica Acta*, 1977, 41(11):1609-1629.
- [77] Stein M, Starinsky A, Katz A, et al. Strontium isotopic, chemical, and sedimentological evidence for the evolution of Lake Lisan and the Dead Sea[J]. *Geochimica et Cosmochimica Acta*, 1997, 61(18):3975-3992.
- [78] Prasad S, Vos H, Nengendank J F W, et al. Evidence from Lake Lisan of solar influence on decadal-to centennial-scale climate variability during marine oxygen isotope stage 2[J]. *Geology*, 2004, 32(7):581-584.
- [79] Yin A, Dang Y Q, Zhang M, et al. Cenozoic tectonic evolution of the Qaidam Basin and its surrounding regions(Part 3):Structural geology, sedimentation, and regional tectonic reconstruction[J]. *Geological Society of America Bulletin*, 2008, 120(7-8):847-876.
- [80] 吴婵, 阎存凤, 李海兵, 等. 柴达木盆地西部新生代构造演化及其对青藏高原北部生长过程的制约[J]. *岩石学报*, 2013, 29(6):2211-2222.
- Wu Chan, Yan Cunfeng, Li Haibing, et al. Cenozoic tectonic evolution of the western Qaidam Basin and its constrain on the growth of the northern Tibetan Plateau[J]. *Acta Petrologica Sinica*, 2013, 29(6):2211-2222.
- [81] Taylor M, Yin A. Active structures of the Himalayan-Tibetan orogen and their relationships to earthquake distribution, contemporary strain field, and Cenozoic volcanism[J]. *Geosphere*, 2009, 5(3):199-214.
- [82] Tapponnier P. Oblique stepwise rise and growth of the Tibet Plateau[J]. *Science*, 2001, 294(5547):1671-1677.
- [83] Xia W, Zhang N, Yuan X, et al. Cenozoic Qaidam Basin, China: A stronger tectonic inverted, extensional rifted basin[J]. *AAPG Bulletin*, 2001, 85(4):715-736.
- [84] Fang X M, Zhang W L, Meng Q, et al. High-resolution magnetostratigraphy of the Neogene Huaitoutala section in the eastern Qaidam Basin on the NE Tibetan Plateau, Qinghai Province, China and its implication on tectonic uplift of the NE Tibetan Plateau[J]. *Earth and Planetary Science Letters*, 2007, 258(1-2):293-306.
- [85] Qiang M, Chen F, Zhang J, et al. Grain size in sediments from Lake Sugan; A possible linkage to dust storm events at the northern margin of the Qinghai-Tibetan Plateau[J]. *Environmental Geology*, 2006, 51(7):1229-1238.
- [86] Meyer B, Tapponnier P, Bourjot L, et al. Crustal thickening in Gansu-Qinghai, lithospheric mantle subduction, and oblique, strike-slip controlled growth of the Tibet Plateau[J]. *Geophysical Journal International*, 1998, 135(1):1-47.
- [87] Métivier F, Gaudemer Y, Tapponnier P, et al. Northeastward growth of the Tibet Plateau deduced from balanced reconstruction of two depositional areas: The Qaidam and Hexi Corridor basins, China[J]. *Tectonics*, 1998, 17(6):823-842.
- [88] Yuan D, Ge W, Chen Z, et al. The growth of northeastern Tibet and its relevance to large-scale continental geodynamics: A review of recent studies[J]. *Tectonics*, 2013, 32(5):1358-1370.
- [89] Lu H, Ye J, Guo L, et al. Towards a clarification of the provenance of Cenozoic sediments in the northern Qaidam Basin[J]. *Lithosphere*, 2018, 11(2):252-272.
- [90] Wang M, Shen Z K. Present-day crustal deformation of Continental China derived from GPS and its tectonic implications[J]. *Journal of Geophysical Research: Solid Earth*, 2020, 125(2):e2019JB018774. doi:10.1029/2019JB018774.
- [91] 杨治林. 柴达木盆地新生代岩相古地理及其演化[M]//中国科学院盐湖研究所. 青海柴达木盆地晚新生代地质环境演化. 北京: 科学出版社, 1986:17-18.
- Yang Zhilin. Cenozoic lithofacies paleogeography and its evolution in Qaidam Basin[M]// Qinghai Institute of Salt Lake, Chinese Academy of Sciences. Evolution of Late Cenozoic Geological Environment in Qaidam Basin, Qinghai Province. Beijing: Science Press. 1986:17-18.

- [92] Lu Y, Fang X, Appel E, et al. A 7.3–1.6 Ma grain size record of interaction between anticline uplift and climate change in the western Qaidam Basin, NE Tibetan Plateau[J]. *Sedimentary Geology*, 2015, 319:40–51. doi:10.1016/j.sedgeo.2015.01.008.
- [93] Liu R, Allen M B, Zhang Q, et al. Basement controls on deformation during oblique convergence: Transpressive structures in the western Qaidam Basin, northern Tibetan Plateau[J]. *Lithosphere*, 2017, 9(4):583–594.
- [94] Wu L, Lin X, Cowgill E, et al. Middle Miocene reorganization of the Altyn Tagh Fault system, northern Tibetan Plateau[J]. *Geological Society of America Bulletin*, 2019, 131(7–8):1157–1178.
- [95] Bally A, Chou I M, Clayton R, et al. Notes on sedimentary basins in China: Report of the American sedimentary basins delegation to the People's Republic of China[R]. US Geological Survey Numbered Series, 1986, 86–327. doi:10.3133/ofr86327.
- [96] Lu Y, Dewald N, Koutsodendris A, et al. Sedimentological evidence for pronounced glacial-interglacial climate fluctuations in NE Tibet in the Latest Pliocene to Early Pleistocene[J]. *Paleoceanography and Paleoclimatology*, 2020, 35(5):PALO20864. doi:10.1029/2020PA003864.
- [97] Zhang W, Appel E, Fang X, et al. Magnetostratigraphy of drill-core SG-1b in the western Qaidam Basin (NE Tibetan Plateau) and tectonic implications[J]. *Geophysical Journal International*, 2014, 197(1):90–118.
- [98] Kaboth-Bahr S, Koutsodendris A, Lu Y, et al. A Late Pliocene to Early Pleistocene (3.3–2.1 Ma) orbital chronology for the Qaidam Basin paleolake (NE Tibetan Plateau) based on the SG-1b drillcore record[J]. *Newsletters on Stratigraphy*, 2020, 53(4):479–496.
- [99] El-Isa Z, Mustafa H. Earthquake deformations in the Lisan deposits and seismotectonic implications[J]. *Geophysical Journal International*, 1986, 86(2):413–424.
- [100] Marco S, Agnon A. Prehistoric earthquake deformations near Masada, Dead Sea Graben[J]. *Geology*, 1995, 23(8):695–698.
- [101] Agnon A, Migowski C, Marco S. Intraclast breccias in laminated sequences reviewed: Recorders of paleo-earthquakes[J]. *Geological Society of America Special Papers*, 2006, 401:195–214. doi:10.1130/2006.2401(13).
- [102] Ken-Tor R, Agnon A, Enzel Y, et al. High-resolution geological record of historic earthquakes in the Dead Sea basin[J]. *Journal of Geophysical Research*, 2001, 106(B2):2221–2234.
- [103] Migowski C, Agnon A, Bookman R, et al. Recurrence pattern of Holocene earthquakes along the Dead Sea transform revealed by varve-counting and radiocarbon dating of lacustrine sediments[J]. *Earth and Planetary Science Letters*, 2004, 222(1):301–314.
- [104] Heifetz E, Agnon A, Marco S. Soft sediment deformation by Kelvin Helmholtz Instability: A case from Dead Sea earthquakes[J]. *Earth and Planetary Science Letters*, 2005, 236(1–2):497–504.
- [105] Wetzler N, Marco S, Heifetz E. Quantitative analysis of seismogenic shear-induced turbulence in lake sediments[J]. *Geology*, 2010, 38(4):303–306.
- [106] Owen G. Load structures: Gravity-driven sediment mobilization in the shallow subsurface[J]. *Geological Society, London, Special Publications*, 2003, 216(1):21–34.
- [107] Avşar U, Jónsson S, Avşar Ö, et al. Earthquake-induced soft-sediment deformations and seismically amplified erosion rates recorded in varved sediments of Köyceğiz Lake (SW Turkey) [J]. *Journal of Geophysical Research: Solid Earth*, 2016, 121(6):4767–4779.
- [108] Monecke K, Anselmetti F S, Becker A, et al. The record of historic earthquakes in lake sediments of Central Switzerland[J]. *Tectonophysics*, 2004, 394(1):21–40.
- [109] Owen G, Moretti M, Alfaro P. Recognising triggers for soft-sediment deformation: Current understanding and future directions [J]. *Sedimentary Geology*, 2011, 235(3–4):133–140.
- [110] Molina J, Alfaro P, Moretti M, et al. Soft-sediment deformation structures induced by cyclic stress of storm waves in tempestites (Miocene, Guadalquivir Basin, Spain) [J]. *Terra Nova*, 1998, 10(3):145–150.
- [111] Moernaut J, Daele M V, Heirman K, et al. Lacustrine turbidites as a tool for quantitative earthquake reconstruction: New evidence for a variable rupture mode in south central Chile[J]. *Journal of Geophysical Research: Solid Earth*, 2014, 119(3):1607–1633.
- [112] Sims J D. Earthquake-induced structures in sediments of Wagoner Norman Lake, San Fernando, California[J]. *Science*, 1973, 182(4108):161–163.
- [113] Alsop G I, Marco S. Seismogenic slump folds formed by gravity-driven tectonics down a negligible subaqueous slope[J]. *Tectonophysics*, 2013, 605:48–69. doi:10.1016/j.tecto.2013.04.004.
- [114] Field M E, Gardner J V, Jennings A E, et al. Earthquake-induced sediment failures on a 0.25° slope, Klamath River delta, California[J]. *Geology*, 1982, 10(10):542–546.
- [115] Schnellmann M, Anselmetti F S, Giardini D, et al. Prehistoric earthquake history revealed by lacustrine slump deposits[J]. *Geology*, 2002, 30(12):1131–1134.
- [116] Shilts W, Clague J J. Documentation of earthquake-induced disturbance of lake sediments using subbottom acoustic profiling[J]. *Canadian Journal of Earth Sciences*, 1992, 29(5):1018–1042.
- [117] Greene H G, Collot J Y, Fisher M A, et al. Neogene tectonic evolution of the new hebrides Island Arc: A review incorporating ODP Drilling Results[J]. *Proceedings of the Ocean Drilling Program, Scientific Results*, 1994, 134:19–46. doi:10.2973/odp.proc.sr.134.002.1994.
- [118] Guo Z J, Yin A, Robinson A, et al. Geochronology and geochemistry of deep-drill-core samples from the basement of the central Tarim Basin[J]. *Journal of Asian Earth Sciences*, 2005, 25(1):45–56.
- [119] Zhang S, Wang D, Liu X, et al. Using borehole core analysis to reveal Late Quaternary paleoearthquakes along the Nankou-Sunhe Fault, Beijing[J]. *Science in China (Series D)*, 2008, 51(8):1154–1168.
- [120] Wald D J, Quitoriano V, Heaton T H, et al. Relationships between peak ground acceleration, peak ground velocity, and

- modified Mercalli intensity in California[J]. *Earthquake Spectra*, 1999, 15(3):557-564.
- [121] Malkawi A I H, Fahmi K J. Locally derived earthquake ground motion attenuation relations for Jordan and conterminous areas[J]. *Quarterly Journal of Engineering Geology and Hydrogeology*, 1996, 29(4):309-319.
- [122] Hough S E, Avni R. The 1170 and 1202 CE Dead Sea Rift earthquakes and long-term magnitude distribution of the Dead Sea Fault Zone[J]. *Israel Journal of Earth Sciences*, 2011, 58(3):295-308.
- [123] Darvazi Y, Agnon A. Calibrating a new attenuation curve for the Dead Sea region using surface wave dispersion surveys in sites damaged by the 1927 Jericho earthquake[J]. *Solid Earth*, 2019, 10(2):379-390.
- [124] Al-Qaryouti M Y. Attenuation relations of peak ground acceleration and velocity in the Southern Dead Sea Transform region[J]. *Arabian Journal of Geosciences*, 2008, 1(2):111-117.
- [125] Wetzler N, Kurzon I. The earthquake activity of Israel: Revisiting 30 years of local and regional seismic records along the Dead Sea Transform[J]. *Seismological Research Letters*, 2016, 87(1):47-58.
- [126] Ferry M, Meghraoui M, Abou Karaki N, et al. Episodic behavior of the Jordan valley section of the Dead Sea Fault inferred from a 14-ka-long integrated catalog of large earthquakes[J]. *Bulletin of the Seismological Society of America*, 2011, 101(1):39-67.
- [127] Meghraoui M. Paleoseismic History of the Dead Sea Fault Zone[J]. *Encyclopedia of Earthquake Engineering*, 2015, doi:10.1007/978-3-642-36197-5_40-1.
- [128] Ambraseys N N. Value of historical records of earthquakes[J]. *Nature*, 1971, 232:375-379. doi:10.1038/232375a0.
- [129] El-Isa Z H, McKnight S, Eaton D. Historical seismicity of the Jordan Dead Sea Transform region and seismotectonic implications [J]. *Arabian Journal of Geosciences*, 2014, 8(6):4039-4055.
- [130] Zohar M, Salamon A, Rubi R. Reappraised list of historical earthquakes that affected Israel and its close surroundings[J]. *Journal of Seismology*, 2016, 20(3):971-985.
- [131] Zohar M. Temporal and spatial patterns of seismic activity associated with the Dead Sea Transform (DST) during the past 3000 yr[J]. *Seismological Research Letters*, 2020, 91(1):207-221.
- [132] Karcz I, Kafri U, Meshel Z. Archaeological evidence for subrecent seismic activity along the Dead Sea-Jordan Rift[J]. *Nature*, 1977, 269(5625):234-235.
- [133] Ellenblum R, Marco S, Agnon A, et al. Crusader castle torn apart by earthquake at dawn, 20 May 1202 [J]. *Geology*, 1998, 26(4):303-306.
- [134] Marco S. Recognition of earthquake-related damage in archaeological sites; Examples from the Dead Sea Fault zone[J]. *Tectonophysics*, 2008, 453(1-4):148-156.
- [135] Begin Z B, Steinberg D M, Ichinose G A, et al. A 40,000 year unchanging seismic regime in the Dead Sea Rift[J]. *Geology*, 2005, 33(4):257-260.
- [136] Kagan E. Multisite Late Quaternary Paleoseismology in the Dead Sea Transform Region: Independent Recording by Lake and Cave Sediments[D]. Jerusalem: The Ph.D. Thesis of Hebrew University, 2011:1-177.
- [137] Hamiel Y, Amit R, Begin Z B, et al. The seismicity along the Dead Sea Fault during the last 60,000 years[J]. *Bulletin of the Seismological Society of America*, 2009, 99(3):2020-2026.
- [138] McCalpin J P. Application of paleoseismic data to seismic hazard assessment and neotectonic research[J]. *International Geophysics*, 2009, 95:1-106. doi:10.1016/S0074-6142(09)95009-4.
- [139] Shao Y, Liu-Zeng J, Oskin M E, et al. Paleoseismic investigation of the Aksay restraining double bend, Altyn Tagh Fault, and its implication for barrier-breaching ruptures[J]. *Journal of Geophysical Research: Solid Earth*, 2018, 123(5):4307-4330.
- [140] Yin A, Rumelhart P E, Butler R, et al. Tectonic history of the Altyn Tagh Fault system in northern Tibet inferred from Cenozoic sedimentation[J]. *Geological Society of America Bulletin*, 2002, 114(10):1257-1295.
- [141] Bendick R, Bilham R, Freymueller J, et al. Geodetic evidence for a low slip rate in the Altyn Tagh Fault system[J]. *Nature*, 2000, 404(6773):69-72.
- [142] Chen Z, Burchfiel B, Liu Y, et al. Global positioning system measurements from eastern Tibet and their implications for India/Eurasia intercontinental deformation[J]. *Journal of Geophysical Research: Solid Earth*, 2000, 105(B7):16215-16227.
- [143] Wagoner Der Woerd J, Tapponnier P, Ryerson J F, et al. Uniform postglacial slip-rate along the central 600 km of the Kunlun Fault (Tibet), from ^{26}Al , ^{10}Be , and ^{14}C dating of riser offsets, and climatic origin of the regional morphology[J]. *Geophysical Journal International*, 2002, 148(3):356-388.
- [144] Piper D J, Shor A N, Clarke J E H. The 1929 "Grand Banks" earthquake, slump, and turbidity current[J]. *Geological Society of America Special Papers*, 1988, 229:77-92. doi:10.1130/SPE229-p77.
- [145] Becker A, Ferry M, Monecke K, et al. Multiarchive paleoseismic record of Late Pleistocene and Holocene strong earthquakes in Switzerland[J]. *Tectonophysics*, 2005, 400(1):153-177.
- [146] Wilhelm B, Nomade J, Crouzet C, et al. Quantified sensitivity of small lake sediments to record historic earthquakes; Implications for paleoseismology[J]. *Journal of Geophysical Research: Earth Surface*, 2016, 121(1):2-16.

SUBAQUEOUS EVENT DEPOSITS RESPONSE TO REGIONAL NEOTECTONICS: CASE STUDIES OF THE DEAD SEA BASIN AND THE Q AidAM BASIN

LU Yin¹, Nadav WETZLER², Shmuel MARCO³, FANG Xiaomin^{4,5}

(1. Department of Geology, University of Innsbruck, Innsbruck 6020, Austria; 2. Geological Survey of Israel, Jerusalem 9692100, Israel; 3. Department of Geophysics, Tel Aviv University, Tel Aviv 6997801, Israel; 4. State Key Laboratory of Tibetan Plateau Earth System, Resources and Environment, Institute of Tibetan Plateau Research (TPESRE), Chinese Academy of Sciences, Beijing 100101; 5. Key Laboratory of Continental Collision and Plateau Uplift, Institute of Tibetan Plateau Research, Chinese Academy of Sciences, Beijing 100101)

Abstract

Sharp changes in lithology and increases in grain size and sedimentation rate of sedimentary sequences from tectonically active basins are often used to indicate regional neotectonic activity. However, these conventional methods have been challenged by others who argue that the sedimentary evidence used to infer tectonism could be climatically induced. Therefore, some form of independent evidence or sedimentary criteria are required to discriminate between these two alternatives.

Seismites, sedimentary structures preserved in lacustrine or marine stratigraphic sequences caused by seismic shaking, are reliable indicators of regional neotectonic activity. Lacustrine/Marine paleoseismology, an emerging cross-field, can extend the record of strong earthquakes and deepen the understanding of fault zone activity by studying seismites preserved in subaqueous sedimentary sequences. In this paper, we use the Dead Sea Basin and Qaidam Basin as examples to understand regional neotectonic activity from the perspective of subaqueous paleoseismology.

The Dead Sea Basin is the deepest and largest continental tectonic structure in the world. A 457 m deep core (ICDP Core 5017-1) was recovered from the Dead Sea depocenter (31°30'29"N, 35°28'16"E) during 2010~2011. The bottom of the core was dated back to 220 ka. *In situ* folded layers and intraclast breccia layer in the core are identified as earthquake indicators, based on their resemblance to the lake outcrop observations of seismites that are known to be earthquake-induced. Based on the Kelvin-Helmholtz instability, we model the ground acceleration needed to produce each seismites by using the physical properties of the Dead Sea deposits. We invert acceleration for earthquake magnitude by considering regional earthquake ground motion attenuation, fault geometry, and other constraints. Based on the magnitude constraints, we develop a 220 ka-long record of $M_w \geq 7$ earthquakes. The record comprises 151 $M_w \geq 7$ events. The record shows a clustered earthquake recurrence pattern and a group-fault temporal clustering model, and reveals an unexpectedly high seismicity rate on a slow-slipping plate boundary.

The Qaidam Basin is the largest topographic depression on the Tibetan Plateau that was formed by the ongoing India-Asia collision. The northeastward growth of the Tibetan Plateau formed a series of sub-parallel NW-SE-trending folds over a distance of ca. 300 km in the western Qaidam Basin. A 723 m deep core was drilled in the basin on the crest of one such fold, the Jianshan Anticline (38°21'9.46"N, 92°16'24.72"E) during 2010~2011. In this study, we focus on the upper 260 m of the core. Paleomagnetic dating constrains the age of the studied core interval to ca. 3.6~1.6 Ma. Sedimentological analysis reveals micro-faults, soft-sediment deformation, slumps, and detachment surfaces preserved in the core interval, which we interpret as paleoearthquake indicators. We recover a 2-Ma seismites sequence comprising 164 $M_w \geq 5$ events. The seismites sequence is relatively more complete during 3.6~2.7 Ma, which comprises 126 events and five seismites clusters. This suggests that the rate of tectonic strain accommodated by the folds/thrusts in the region varies in time and thus reveals episodic local deformation. During the clusters, regional deformation is concentrated more in the fold-and-thrust system than along regional major strike-slip faults.

Key words: seismites; lacustrine/marine event deposits; lacustrine/marine paleoseismology; earthquake recurrence pattern; regional deformation